

Supporting Information:

**Atomistic Insight into Screening and Role of Oxygen in Enhancing Li⁺
Conductivity of Li₇P₃S_{11-x}O_x Solid-State Electrolytes**

Hanghui Liu,^{a,b} Zhenhua Yang,^{*a,b} Qun Wang,^{a,b} Xianyou Wang^c and Xingqiang Shi^d

^a *Key Laboratory of Materials Design and Preparation Technology of Hunan Province, School of Materials Science and Engineering, Xiangtan University, Xiangtan 411105, Hunan, China*

^b *Key Laboratory of Low Dimensional Materials & Application Technology (Ministry of Education), School of Materials Science and Engineering, Xiangtan University, Xiangtan 411105, Hunan, China*

^c *National Local Joint Engineering Laboratory for Key Materials of New Energy Storage Battery, National Base for International Science & Technology Cooperation, Hunan Province Key Laboratory of Electrochemical Energy Storage & Conversion, School of Chemistry, Xiangtan University, Xiangtan 411105, Hunan, China*

^d *Department of Physics, Southern University of Science and Technology, Shenzhen 518055, China*

*Corresponding authors. E-mail addresses: yangzhenhua@xtu.edu.cn (Zhenhua Yang).

1. Electronic Band Structure of $\text{Li}_7\text{P}_3\text{S}_{11}$

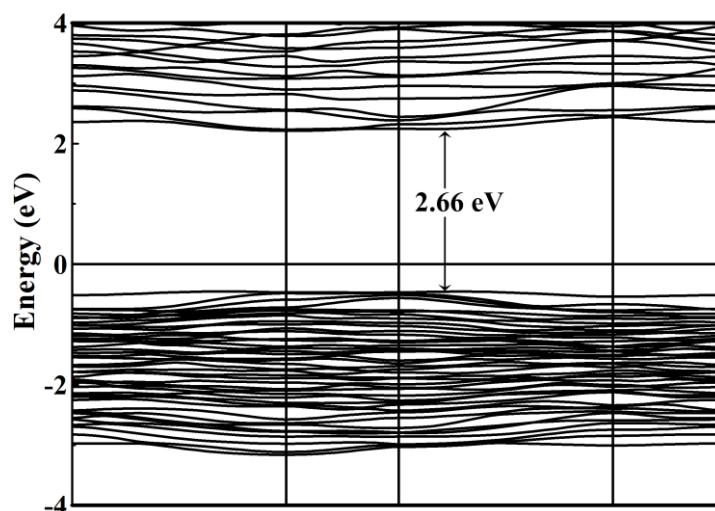


Fig. S1 Electronic band structure of $\text{Li}_7\text{P}_3\text{S}_{11}$ supercell in non-spin polarized configuration.

2. Structural Screening Process for Oxygen Doped $\text{Li}_7\text{P}_3\text{S}_{11}$

We labeled O_s , 2O_s , 3O_s and 4O_s as the structures of $\text{Li}_7\text{P}_3\text{S}_{10.75}\text{O}_{0.25}$, $\text{Li}_7\text{P}_3\text{S}_{10.50}\text{O}_{0.50}$, $\text{Li}_7\text{P}_3\text{S}_{10.25}\text{O}_{0.75}$ and $\text{Li}_7\text{P}_3\text{S}_{10}\text{O}$, respectively. In order to obtain the most stable structures of $\text{Li}_7\text{P}_3\text{S}_{10.75}\text{O}_{0.25}$, $\text{Li}_7\text{P}_3\text{S}_{10.50}\text{O}_{0.50}$, $\text{Li}_7\text{P}_3\text{S}_{10.25}\text{O}_{0.75}$ and $\text{Li}_7\text{P}_3\text{S}_{10}\text{O}$, we calculated their relative energies of each possible structure for $\text{Li}_7\text{P}_3\text{S}_{11-x}\text{O}_x$ ($x = 0.25, 0.50, 0.75$ and 1). After structural search, the optimum structures of $\text{Li}_7\text{P}_3\text{S}_{10.75}\text{O}_{0.25}$, $\text{Li}_7\text{P}_3\text{S}_{10.50}\text{O}_{0.50}$, $\text{Li}_7\text{P}_3\text{S}_{10.25}\text{O}_{0.75}$ and $\text{Li}_7\text{P}_3\text{S}_{10}\text{O}$ turn out, as shown in Fig. S18.

2.1. O_s ($\text{Li}_7\text{P}_3\text{S}_{10.75}\text{O}_{0.25}$)

O_s ($\text{Li}_7\text{P}_3\text{S}_{10.75}\text{O}_{0.25}$) is created by replacing one S with O and the numbers of different S sites are labeled as 1-11 (see Fig. S2a). We calculated the relative energy values of O_s ($\text{Li}_7\text{P}_3\text{S}_{10.75}\text{O}_{0.25}$) with different oxygen-sulfur substitution to find the most favorable O-doping site (see Fig. S2b). As seen from Fig. S3, it can be found

that the most stable S site is site 1.

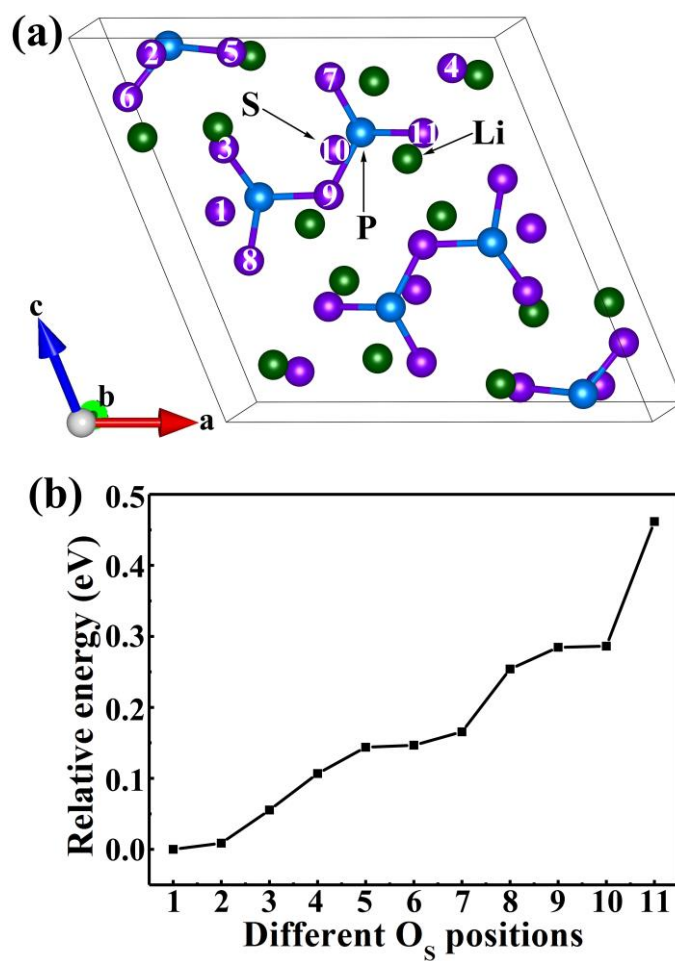


Fig. S2 (a) Eleven kinds of S sites in $\text{Li}_7\text{P}_3\text{S}_{11}$. (b) Relative energy as a function of O_s position.

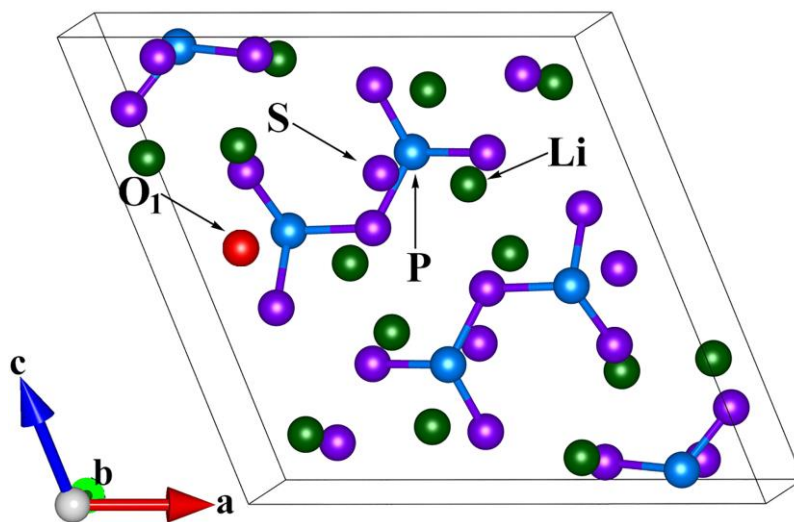


Fig. S3 Ball-and-stick model of O_s ($\text{Li}_7\text{P}_3\text{S}_{10.75}\text{O}_{0.25}$).

2.2. $2O_s$ ($Li_7P_3S_{10.5}O_{0.5}$)

Now, we further discussed the possible structure of $2O_s$ ($Li_7P_3S_{10.5}O_{0.5}$). Firstly, we labeled O-doping site as 1 and we also labeled other S sites as numbers (2-44) in the crystal structure of O_s ($Li_7P_3S_{10.75}O_{0.25}$) (see Fig. S4). Subsequently, according to structural symmetry, all atomic configurations of $2O_s$ ($Li_7P_3S_{10.5}O_{0.5}$) were selected to find another favorable O-doping site based on the structure of O_s ($Li_7P_3S_{10.75}O_{0.25}$) (Fig. S5a) and the corresponding relative energies as a function of the distances between O_1 and another O were also calculated (Fig. S5b). As presented in Fig. S5b, it is obvious that the relative energy of $2O_s$ ($Li_7P_3S_{10.5}O_{0.5}$) tend to distribute symmetrically with increasing the distance between possible O-doping site and O_1 . Position 2 is likely to the next doping site due to its smallest relative energy. Accordingly, the most stable structure of $2O_s$ ($Li_7P_3S_{10.5}O_{0.5}$) is presented in Fig. S6.

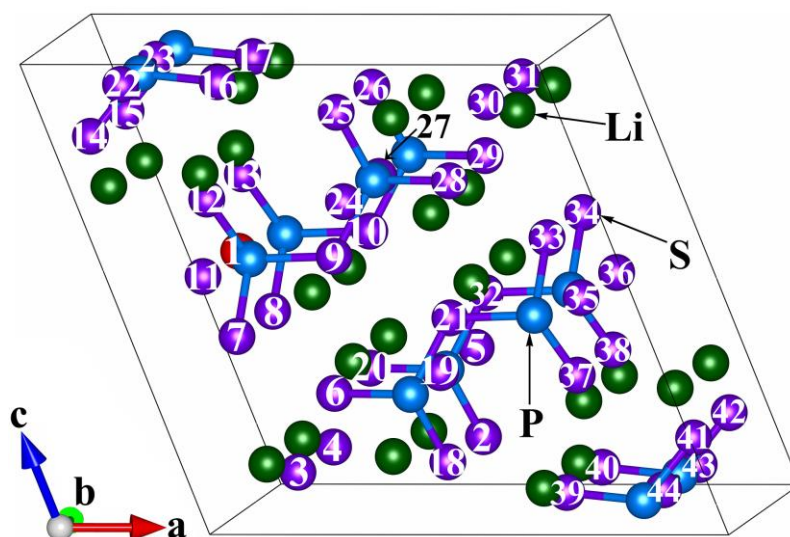


Fig. S4 The crystal structure of O_s ($Li_7P_3S_{10.75}O_{0.25}$). Here, O-doping site is labeled as 1 and other S sites are also labeled as numbers (2-44).

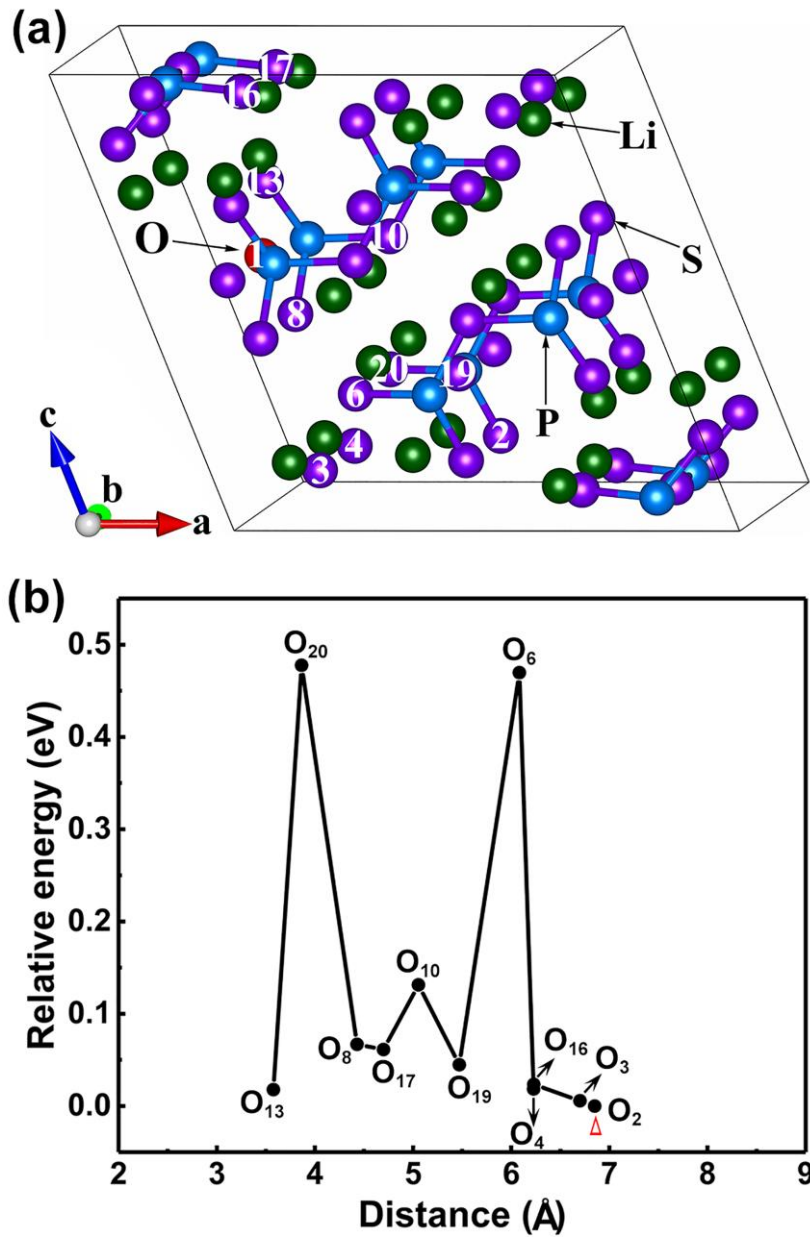


Fig. S5 (a) The crystal structure of O_s ($Li_7P_3S_{10.75}O_{0.25}$) with several kinds of possible O-doping sites. (b) The relative energy of $2O_s$ ($Li_7P_3S_{10.50}O_{0.50}$) as a function of the distance between O_1 and another O.

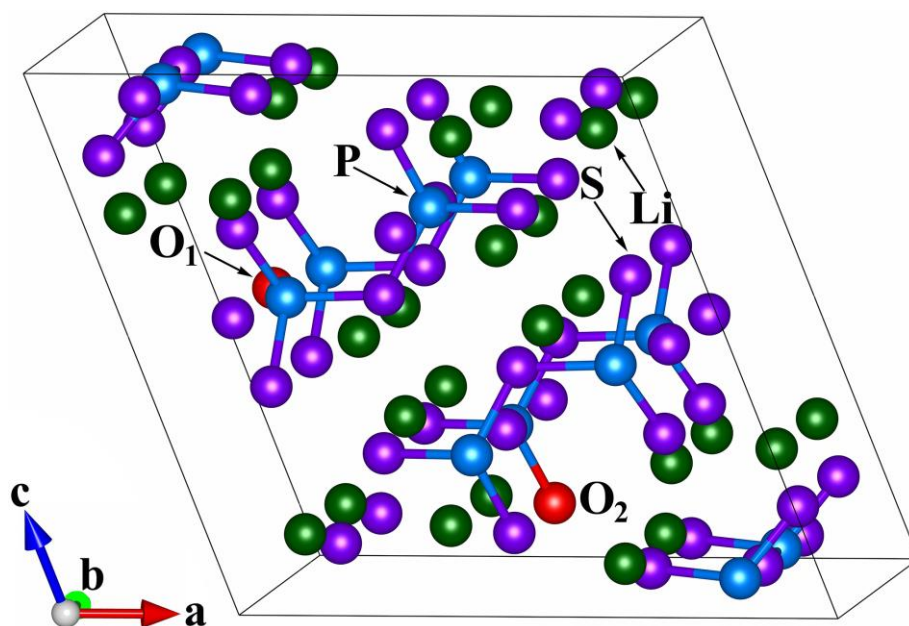


Fig. S6 Ball-and-stick model of $2O_s$ ($Li_7P_3S_{10.50}O_{0.50}$).

2.3. $3O_s$ ($Li_7P_3S_{10.25}O_{0.75}$)

Furthermore, the possible structures of $3O_s$ ($Li_7P_3S_{10.25}O_{0.75}$) are further considered. Firstly, we labeled O-doping sites as 1 and 2. We also labeled other S sites as numbers (3-44) in the crystal structure of $2O_s$ ($Li_7P_3S_{10.50}O_{0.50}$) (see Fig. S7). Similarly, according to structural symmetry, all atomic configurations of $3O_s$ ($Li_7P_3S_{10.25}O_{0.75}$) were selected to find another favorable O-doping site based on the structure of $2O_s$ ($Li_7P_3S_{10.50}O_{0.50}$) (see Fig. S8a) and the corresponding relative energies as a function of the distances between O_1 and another O were also calculated (see Fig. S8b). It is clear that the relative energy of $3O_s$ ($Li_7P_3S_{10.25}O_{0.75}$) tend to distribute symmetrically with increasing distance between possible O-doping site and O_1 . The same phenomenon can be observed with increasing distances between possible O-doping sites and O_2 (see Fig. S9). Site 3 is most likely to be occupied by next oxygen due to the smallest relative energy.

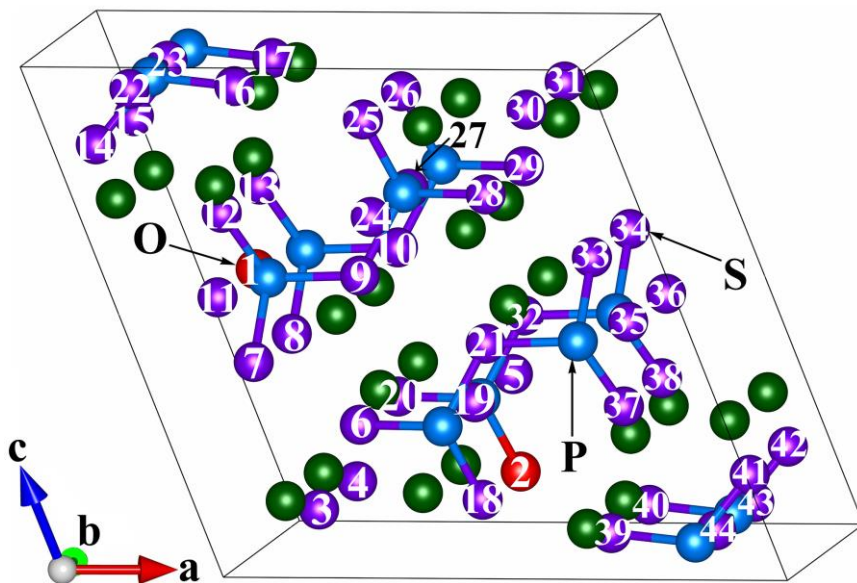


Fig. S7 The crystal structure of $2O_s$ ($Li_7P_3S_{10.5}O_{0.50}$). Here, O-doping sites are labeled as 1 and 2. Other S sites are also labeled as numbers (3-44).

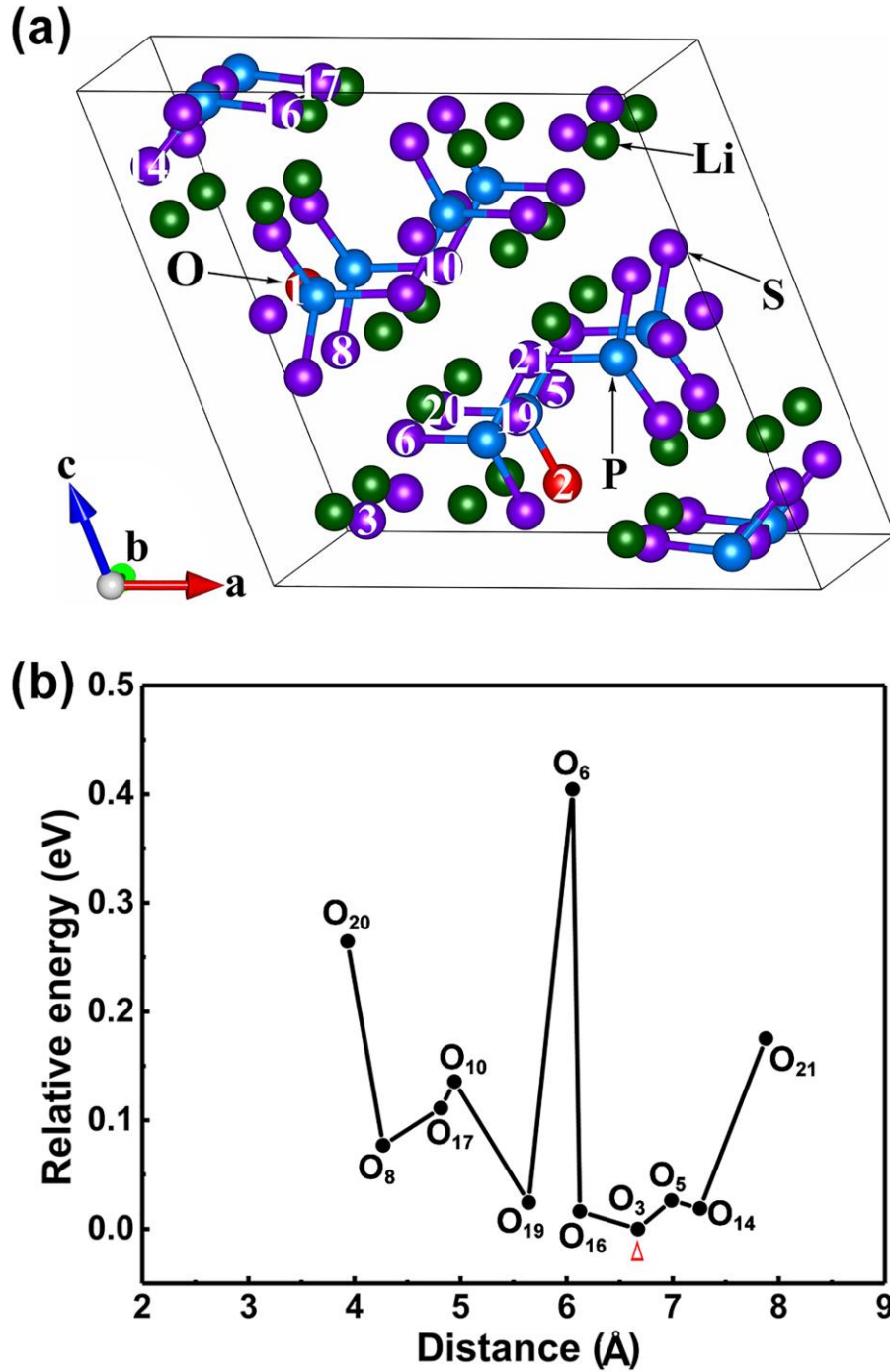


Fig. S8 (a) The crystal structure of $2O_S$ ($Li_7P_3S_{10.5}O_{0.50}$). Here, we considered next possible O-doping sites and they were labeled as numbers; (b) The relative energy of $3O_S$ ($Li_7P_3S_{10.25}O_{0.75}$) as a function of the distance between O_1 and another O.

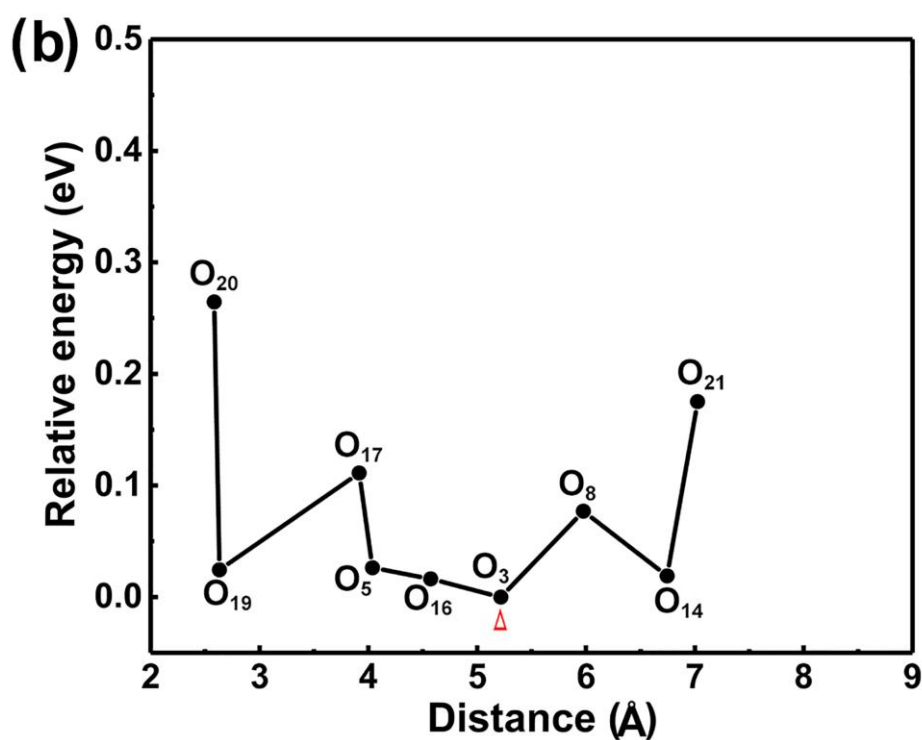
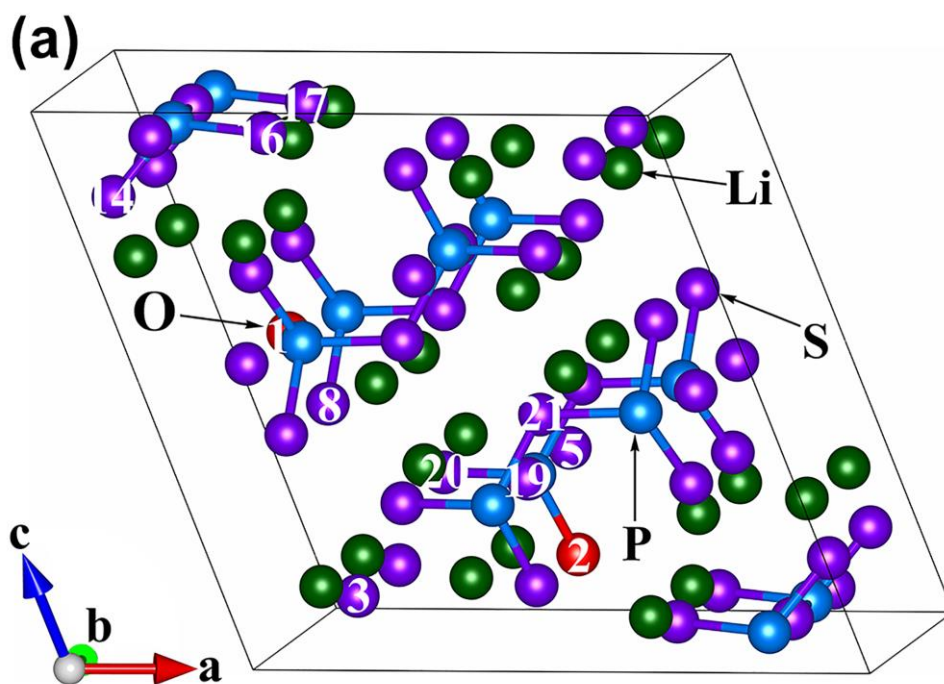


Fig. S9 (a) The crystal structure of $2O_s$ ($Li_7P_3S_{10.5}O_{0.50}$). Here, we considered next possible O-doping sites and they were labeled as numbers; (b) The relative energy of $3O_s$ ($Li_7P_3S_{10.25}O_{0.75}$) as a function of the distance between O_2 and another O.

Next, the relaxed and unrelaxed structures of $3O_s$ ($Li_7P_3S_{10.25}O_{0.75}$) were further compared and analyzed (see Fig. S10). Interestingly, three oxygen atoms tend to be in form of isosceles triangular after structural optimization. Accordingly, the most stable structure of $3O_s$ ($Li_7P_3S_{10.25}O_{0.75}$) is presented in Fig. S11.

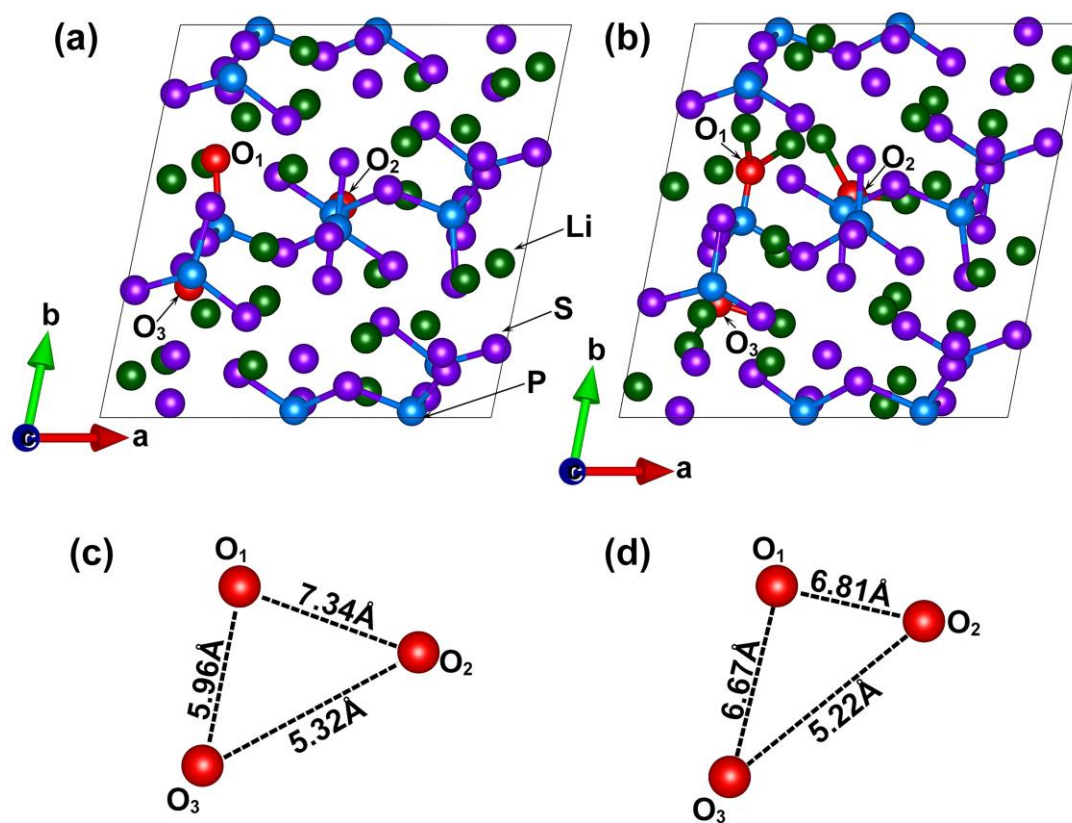


Fig. S10 Ball and stick models of $3O_s$ (a) before structural optimization and (b) after structural optimization. Local atomic models of $3O_s$ (c) before structural optimization and (d) after structural optimization.

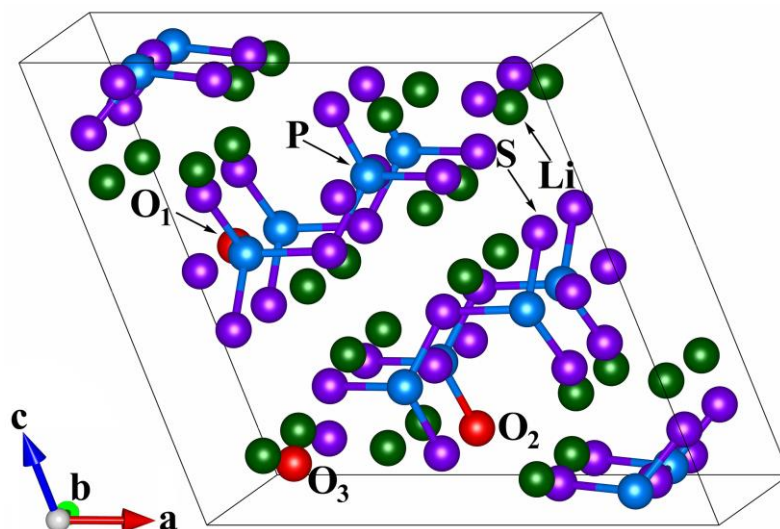


Fig. S11 Ball-and-stick model of $3O_S$ ($\text{Li}_7\text{P}_3\text{S}_{10.25}\text{O}_{0.75}$).

2.4. $4O_S$ ($\text{Li}_7\text{P}_3\text{S}_{10}\text{O}$)

Firstly, we labeled O-doping site as 1, 2 and 3. We also labeled other S sites as numbers (4-44) in the crystal structure of $3O_S$ ($\text{Li}_7\text{P}_3\text{S}_{10.25}\text{O}_{0.75}$) (see Fig. S12). Similarly, according to structural symmetry, all atomic configurations of $4O_S$ ($\text{Li}_7\text{P}_3\text{S}_{10}\text{O}$) were selected to find the another favorable O-doping site based on the structure of $3O_S$ ($\text{Li}_7\text{P}_3\text{S}_{10.25}\text{O}_{0.75}$) and the corresponding relative energies as a function of the distances between O_1 (O_2 , O_3) and another O were also calculated (see Fig. S13-S15). Site 4 is most likely to be occupied by next oxygen due to the smallest relative energy.

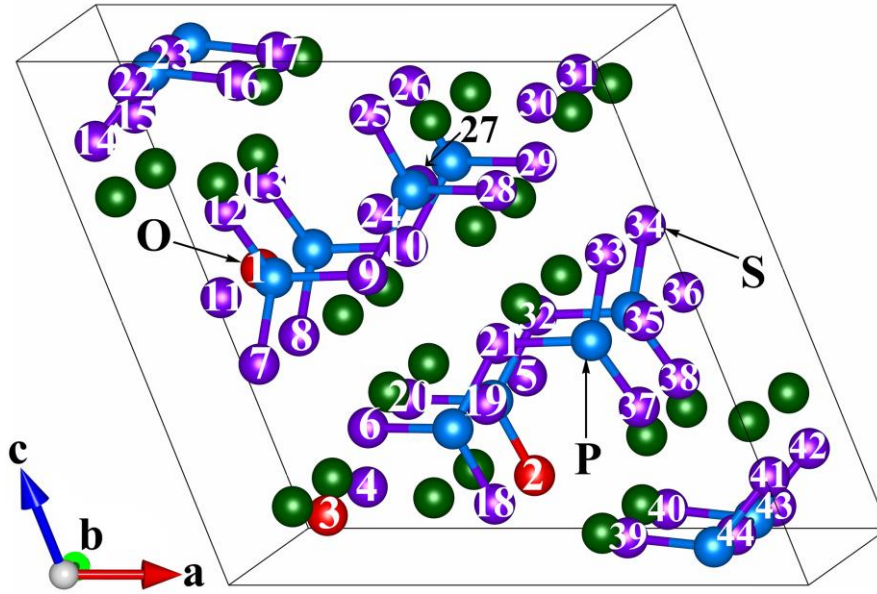


Fig. S12 The crystal structure of $3O_S$ ($Li_7P_3S_{10.25}O_{0.75}$). Here, O-doping sites are labeled as 1, 2 and 3. Other S sites are also labeled as numbers (4-44).

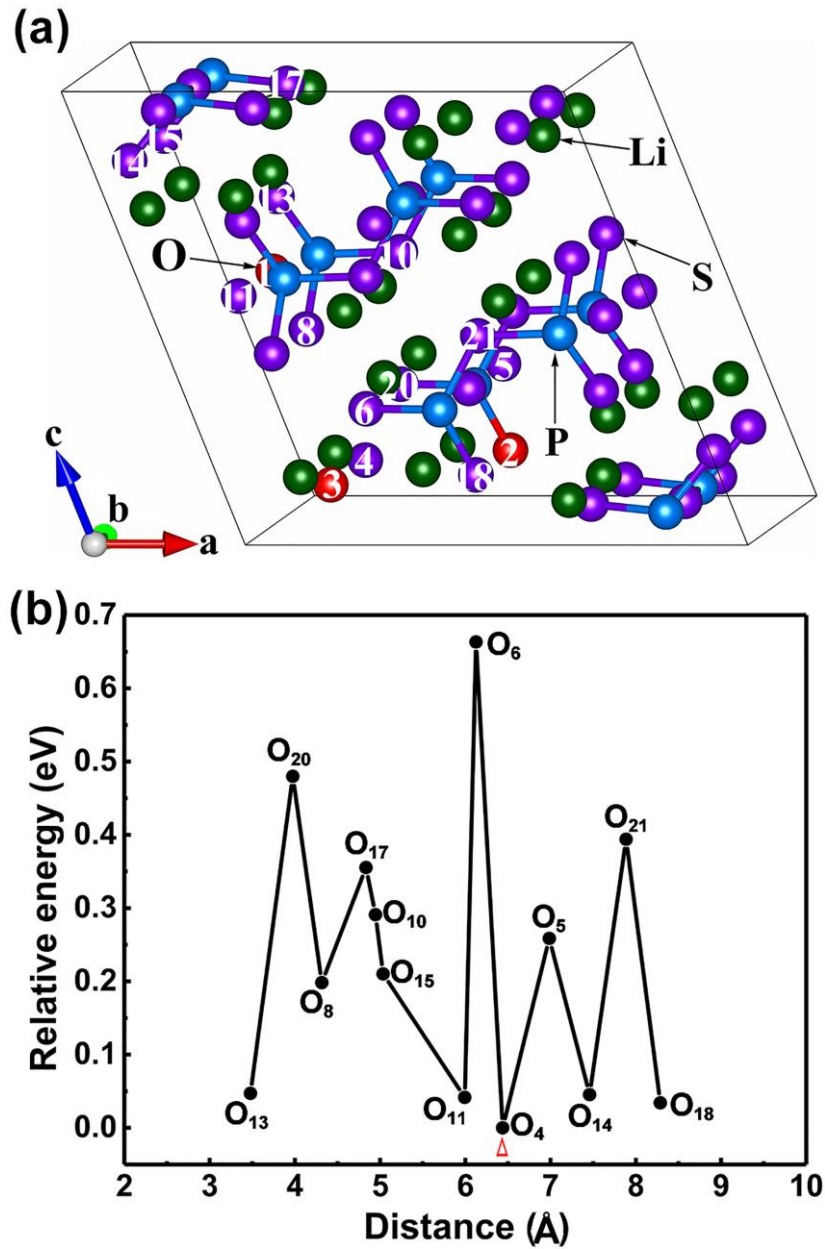


Fig. S13 (a) The crystal structure of $3O_s$ ($Li_7P_3S_{10.25}O_{0.75}$). Here, we considered next possible O-doping sites and they were labeled as numbers; (b) The relative energy of $4O_s$ ($Li_7P_3S_{10}O$) as a function of the distance between O_1 and another O.

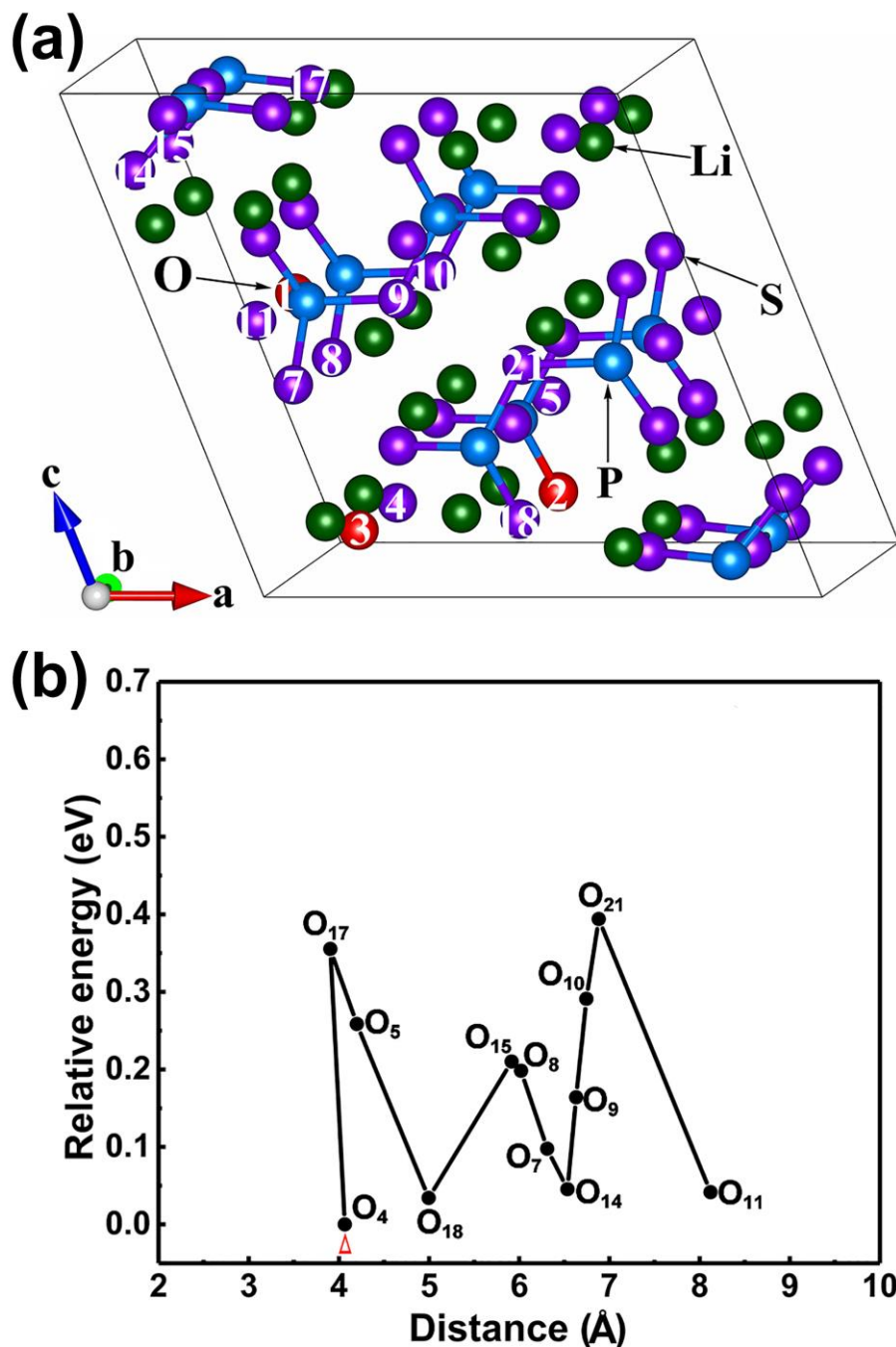


Fig. S14 (a) The crystal structure of $3O_s$ ($Li_7P_3S_{10.25}O_{0.75}$). Here, we considered next possible O-doping sites and they were labeled as numbers; (b) The relative energy of $4O_s$ ($Li_7P_3S_{10}O$) as a function of the distance between O_2 and another O.

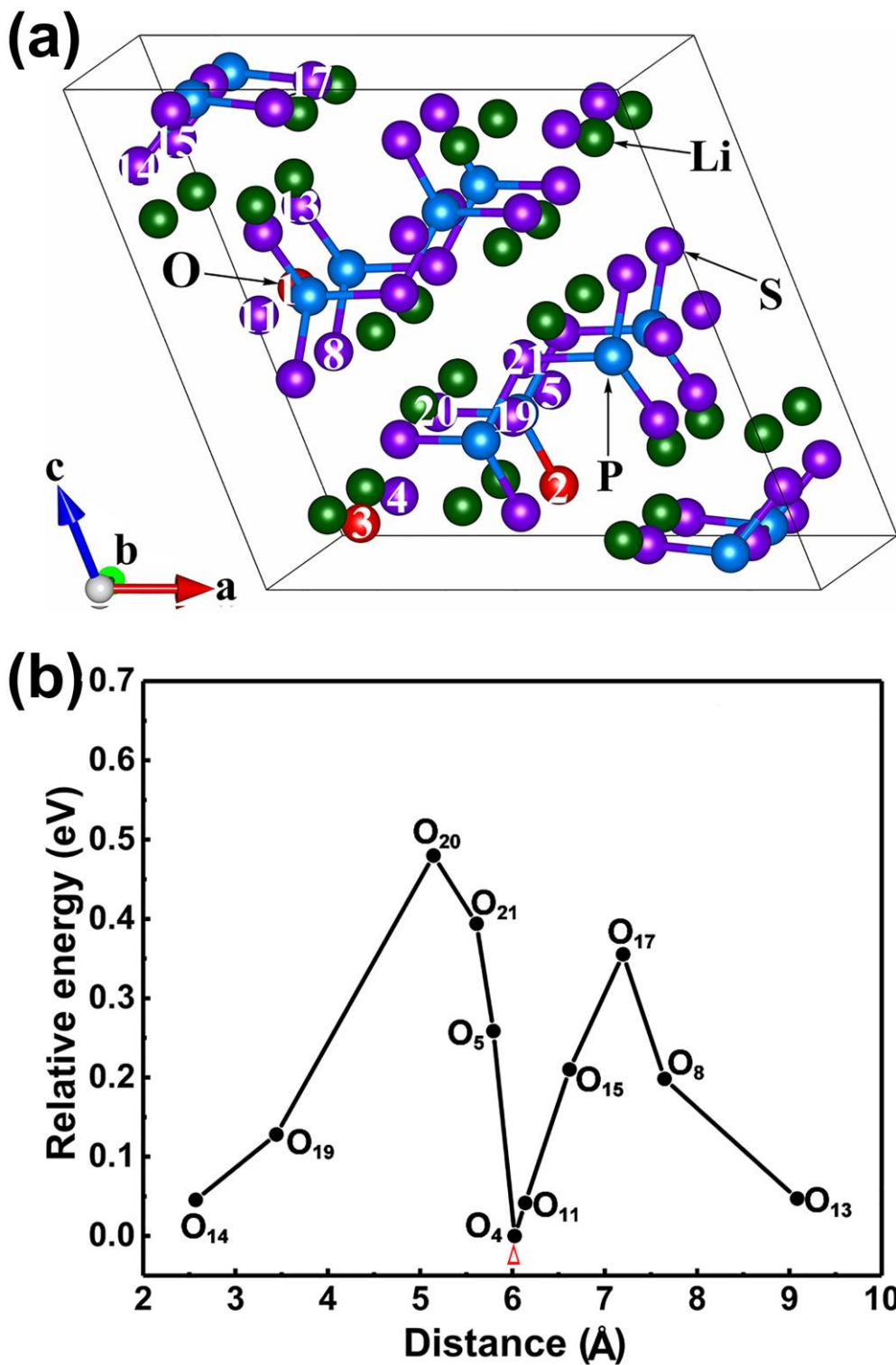


Fig. S15 (a) The crystal structure of $3O_S$ ($Li_7P_3S_{10.25}O_{0.75}$). Here, we considered next possible O-doping sites and they were labeled as numbers; (b) The relative energy of $4O_S$ ($Li_7P_3S_{10}O$) as a function of the distance between O_3 and another O.

Next, the relaxed and unrelaxed structures of $4O_s$ ($Li_7P_3S_{10}O$) were further compared and analyzed (see Fig. S16). Interestingly, four oxygen atoms tend to be more regularly distributed in the structure after structural optimization. Accordingly, the most stable structure of $4O_s$ ($Li_7P_3S_{11}O$) is presented in Fig. S17.

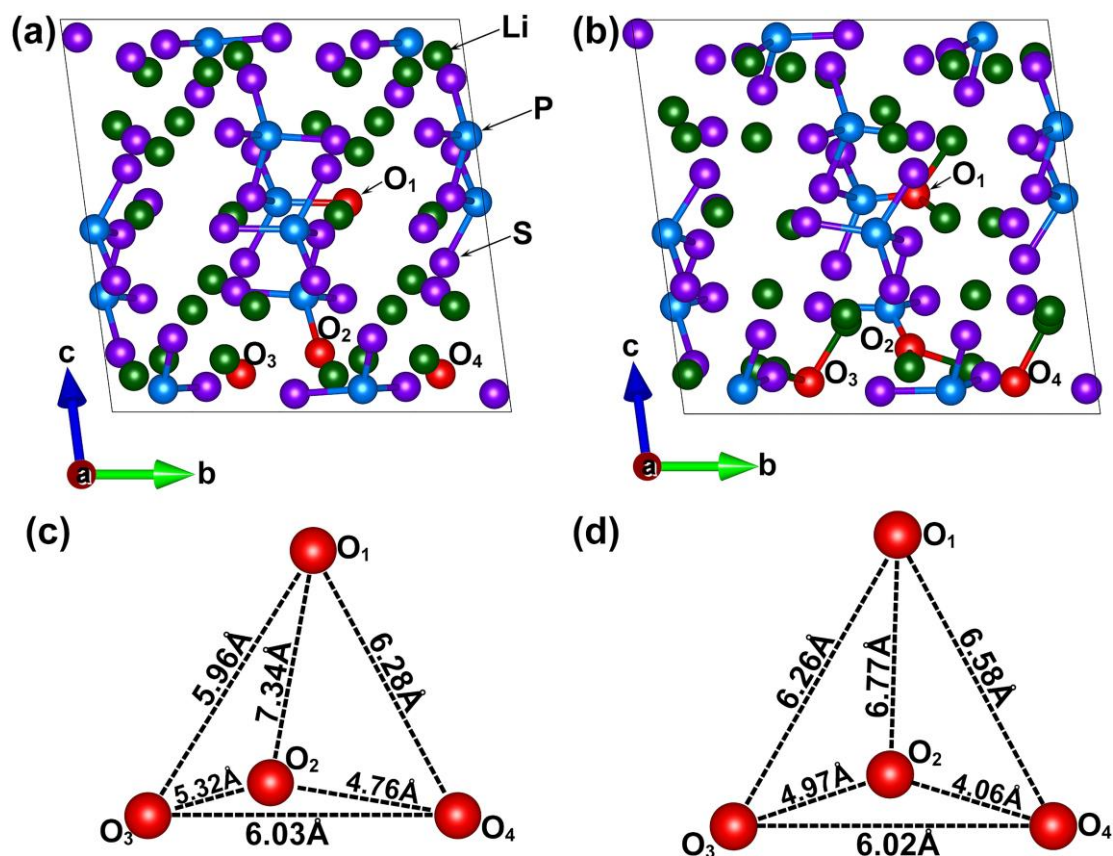


Fig. S16 Ball and stick models of $4O_s$ (a) before structural optimization and (b) after structural optimization. Local atomic models of $4O_s$ (c) before structural optimization and (d) after structural optimization.

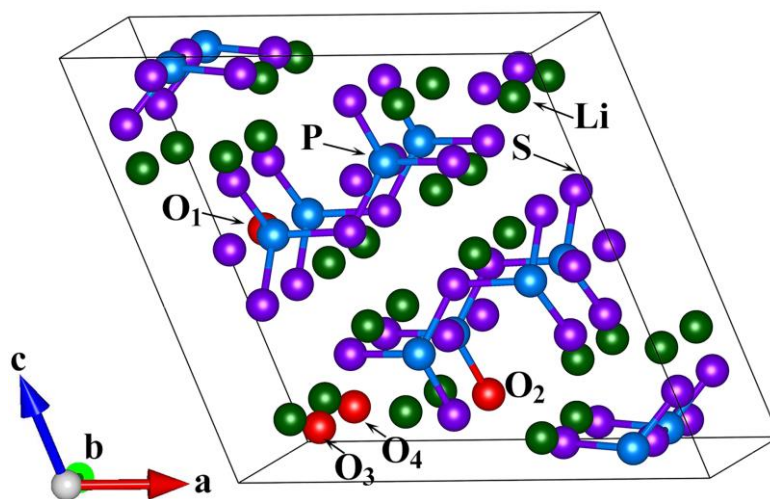


Fig. S17 Ball-and-stick model of $4O_s$ ($\text{Li}_7\text{P}_3\text{S}_{10}\text{O}$).

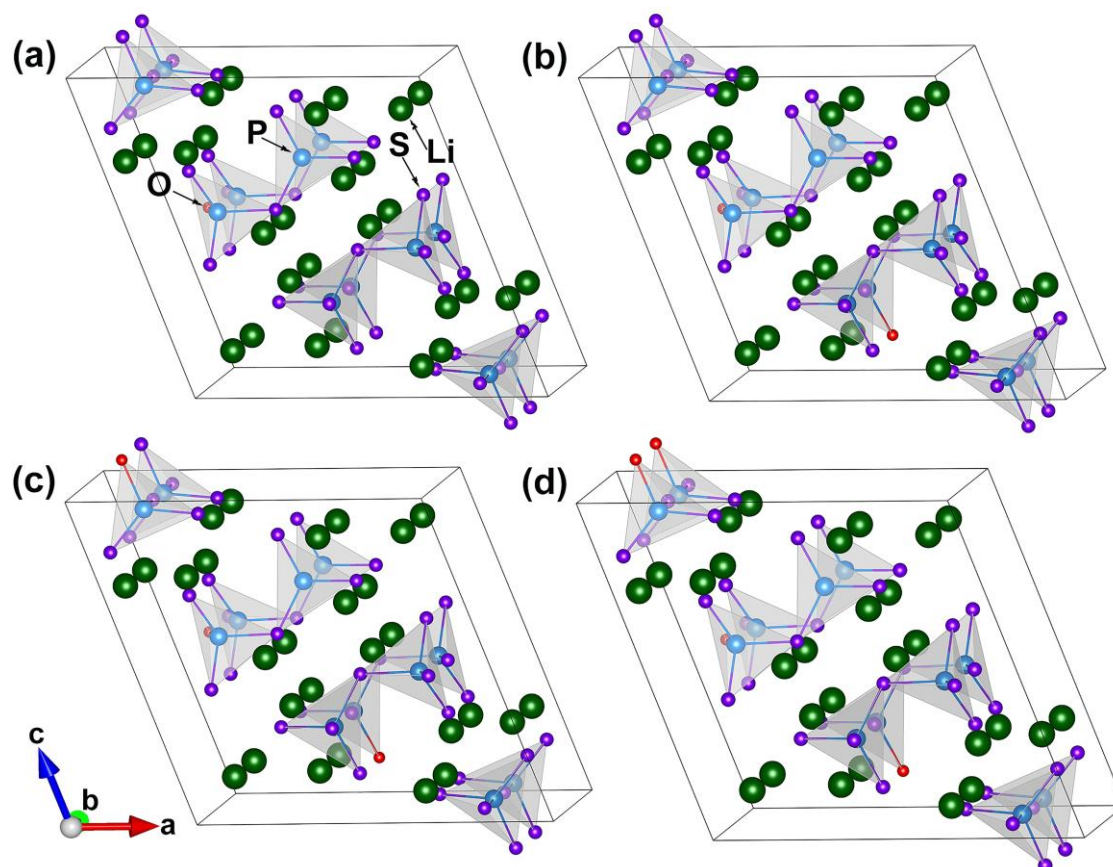


Fig. S18 The optimum structures for (a) $\text{Li}_7\text{P}_3\text{S}_{10.75}\text{O}_{0.25}$, (b) $\text{Li}_7\text{P}_3\text{S}_{10.50}\text{O}_{0.50}$, (c) $\text{Li}_7\text{P}_3\text{S}_{10.25}\text{O}_{0.75}$ and (d) $\text{Li}_7\text{P}_3\text{S}_{10}\text{O}$.

3. Investigation of Impurity Formation Energies

Table S1. Crystal Structure and Calculated Formation Enthalpies of Phases in the Li-P-S System

phase	structure	GGA	ref	phase	structure	GGA	ref
Li ₃ P ₇	<i>P2₁2₁2₁</i>	-3.88	-4.62 ¹	Li ₃ P	<i>P6₃/mmc</i>	-2.86	-2.94 ¹
LiP	<i>P2₁/c</i>	-1.09	-1.19 ¹	Li ₂ S	<i>Fm$\bar{3}m$</i>	-4.05	
LiP ₇	<i>I4₁/acd</i>	-1.52	-2.26 ¹	P ₄ S ₃	<i>Pnma</i>	-1.17	
P ₄ S ₄	<i>C12/c1</i>	-1.25		P ₄ S ₆	<i>P2₁/c1</i>	-1.79	
P ₄ S ₇	<i>P12₁/c1</i>	-2.13		P ₄ S ₉	<i>Ia3</i>	-2.37	
P ₄ S ₁₀	<i>P1</i>	-2.45		P ₄ S ₅	<i>P2₁</i>	-1.61	
LiP ₅	<i>Pna2₁</i>	-1.35	-1.87 ¹	P ₂ S ₃	<i>P2₁/c</i>	-0.90	
P ₂ S ₅	<i>P1</i>	-1.24		P ₄ S ₇	<i>P1</i>	-1.21	
PS	<i>P1</i>	-0.32					

Table S2. Crystal Structures and Calculated Formation Enthalpies of Oxides

phase	structure	GGA	ref	exp	phase	structure	GGA	ref
Li ₂ S ₂ O ₇	<i>Pnma</i>	-22.40			Li ₂ SO ₄	<i>P2₁/c</i>	-15.85	
Li ₃ PO ₄	<i>Pmn2₁</i>	-21.77	-22.19 ¹		Li ₆ P ₆ O ₁₈	<i>P2₁/n</i>	-79.66	
Li ₄ P ₂ O ₇	<i>P2₁/c</i>	-35.19	-36.02 ¹		LiPO ₃	<i>P2/c</i>	-13.28	-13.69 ¹
Li ₂ O ₂	<i>P6₃/mmc</i>	-6.88	-7.04 ¹	-6.56 ²	P ₄ S ₄ O ₆	<i>I4c2</i>	-20.95	
Li ₂ O	<i>Fm$\bar{3}m$</i>	-6.16	-6.28 ¹	-6.21 ²	P ₄ S ₃ O ₆	<i>P12₁/c1</i>	-20.68	
P ₄ S ₆ O ₃	<i>P12₁/m1</i>	-11.67			P ₄ S ₂ O ₆	<i>P12₁/c1</i>	-20.27	
P ₄ SO ₆	<i>P12₁/c1</i>	-19.74			P ₄ SO ₇	<i>P1</i>	-22.89	
P ₄ O ₇	<i>P2₁/c</i>	-22.84	-24.03 ¹		P ₂ O ₅	<i>Pnma</i>	-16.59	-17.34 ¹
P ₄ O ₉	<i>R$\bar{3}c$</i>	-29.84	-31.27 ¹		P ₄ O ₆	<i>P2₁/m</i>	-19.09	-20.17 ¹
P ₄ O ₈	<i>C2/c</i>	-26.48	-27.79 ¹		SO ₂	<i>Aba2</i>	-4.365	
S ₈ O	<i>Pca2₁</i>	-1.724			S ₃ O ₉	<i>P2₁nb</i>	-17.99	
SO ₃	<i>Pna2₁</i>	-5.996						

Table S3. Constraint Conditions for Chemical Potentials of Oxygen about Oxides

Oxides	Constraint Relation	Bounded Value
Li ₃ PO ₄	$3\Delta\mu_{\text{Li}} + \Delta\mu_{\text{P}} + 4\Delta\mu_{\text{O}} = \Delta H_f(\text{Li}_3\text{PO}_4)$	$\Delta\mu_{\text{O}} = -4.11 \text{ eV}$
Li ₂ S ₂ O ₇	$2\Delta\mu_{\text{Li}} + 2\Delta\mu_{\text{S}} + 7\Delta\mu_{\text{O}} = \Delta H_f(\text{Li}_2\text{S}_2\text{O}_7)$	$\Delta\mu_{\text{O}} = -2.69 \text{ eV}$
LiPO ₃	$\Delta\mu_{\text{Li}} + \Delta\mu_{\text{P}} + 3\Delta\mu_{\text{O}} = \Delta H_f(\text{LiPO}_3)$	$\Delta\mu_{\text{O}} = -3.83 \text{ eV}$
Li ₂ SO ₄	$2\Delta\mu_{\text{Li}} + \Delta\mu_{\text{S}} + 4\Delta\mu_{\text{O}} = \Delta H_f(\text{Li}_2\text{SO}_4)$	$\Delta\mu_{\text{O}} = -3.07 \text{ eV}$
Li ₆ P ₆ O ₁₈	$6\Delta\mu_{\text{Li}} + 6\Delta\mu_{\text{P}} + 18\Delta\mu_{\text{O}} = \Delta H_f(\text{Li}_6\text{P}_6\text{O}_{18})$	$\Delta\mu_{\text{O}} = -3.83 \text{ eV}$
Li ₄ P ₂ O ₇	$4\Delta\mu_{\text{Li}} + 2\Delta\mu_{\text{P}} + 7\Delta\mu_{\text{O}} = \Delta H_f(\text{Li}_4\text{P}_2\text{O}_7)$	$\Delta\mu_{\text{O}} = -4.01 \text{ eV}$
Li ₂ O	$2\Delta\mu_{\text{Li}} + \Delta\mu_{\text{O}} = \Delta H_f(\text{Li}_2\text{O})$	$\Delta\mu_{\text{O}} = -2.60 \text{ eV}$
Li ₂ O ₂	$2\Delta\mu_{\text{Li}} + 2\Delta\mu_{\text{O}} = \Delta H_f(\text{Li}_2\text{O}_2)$	$\Delta\mu_{\text{O}} = -1.66 \text{ eV}$
P ₄ S ₃ O ₆	$4\Delta\mu_{\text{P}} + 3\Delta\mu_{\text{S}} + 6\Delta\mu_{\text{O}} = \Delta H_f(\text{P}_4\text{S}_3\text{O}_6)$	$\Delta\mu_{\text{O}} = -3.45 \text{ eV}$
P ₄ S ₆ O ₃	$4\Delta\mu_{\text{P}} + 6\Delta\mu_{\text{S}} + 3\Delta\mu_{\text{O}} = \Delta H_f(\text{P}_4\text{S}_6\text{O}_3)$	$\Delta\mu_{\text{O}} = -3.89 \text{ eV}$
P ₄ SO ₆	$4\Delta\mu_{\text{P}} + \Delta\mu_{\text{S}} + 6\Delta\mu_{\text{O}} = \Delta H_f(\text{P}_4\text{SO}_6)$	$\Delta\mu_{\text{O}} = -3.29 \text{ eV}$
P ₄ SO ₇	$4\Delta\mu_{\text{P}} + \Delta\mu_{\text{S}} + 7\Delta\mu_{\text{O}} = \Delta H_f(\text{P}_4\text{SO}_7)$	$\Delta\mu_{\text{O}} = -3.27 \text{ eV}$
P ₄ S ₂ O ₆	$4\Delta\mu_{\text{P}} + 2\Delta\mu_{\text{S}} + 6\Delta\mu_{\text{O}} = \Delta H_f(\text{P}_4\text{S}_2\text{O}_6)$	$\Delta\mu_{\text{O}} = -3.38 \text{ eV}$
P ₄ S ₄ O ₆	$4\Delta\mu_{\text{P}} + 4\Delta\mu_{\text{S}} + 6\Delta\mu_{\text{O}} = \Delta H_f(\text{P}_4\text{S}_4\text{O}_6)$	$\Delta\mu_{\text{O}} = -3.49 \text{ eV}$
P ₂ O ₅	$2\Delta\mu_{\text{P}} + 5\Delta\mu_{\text{O}} = \Delta H_f(\text{P}_2\text{O}_5)$	$\Delta\mu_{\text{O}} = -3.32 \text{ eV}$
P ₄ O ₆	$4\Delta\mu_{\text{P}} + 6\Delta\mu_{\text{O}} = \Delta H_f(\text{P}_4\text{O}_6)$	$\Delta\mu_{\text{O}} = -3.18 \text{ eV}$
P ₄ O ₇	$4\Delta\mu_{\text{P}} + 7\Delta\mu_{\text{O}} = \Delta H_f(\text{P}_4\text{O}_7)$	$\Delta\mu_{\text{O}} = -3.26 \text{ eV}$
P ₄ O ₈	$4\Delta\mu_{\text{P}} + 8\Delta\mu_{\text{O}} = \Delta H_f(\text{P}_4\text{O}_8)$	$\Delta\mu_{\text{O}} = -3.31 \text{ eV}$
P ₄ O ₉	$4\Delta\mu_{\text{P}} + 9\Delta\mu_{\text{O}} = \Delta H_f(\text{P}_4\text{O}_9)$	$\Delta\mu_{\text{O}} = -3.32 \text{ eV}$

S_3O_9	$3\Delta\mu_S + 9\Delta\mu_O = \Delta H_f(S_3O_9)$	$\Delta\mu_O = -2.00 \text{ eV}$
S_8O	$8\Delta\mu_S + \Delta\mu_O = \Delta H_f(S_8O)$	$\Delta\mu_O = -1.72 \text{ eV}$
SO_2	$\Delta\mu_S + 2\Delta\mu_O = \Delta H_f(SO_2)$	$\Delta\mu_O = -2.18 \text{ eV}$
SO_3	$\Delta\mu_S + 3\Delta\mu_O = \Delta H_f(SO_3)$	$\Delta\mu_O = -2.00 \text{ eV}$

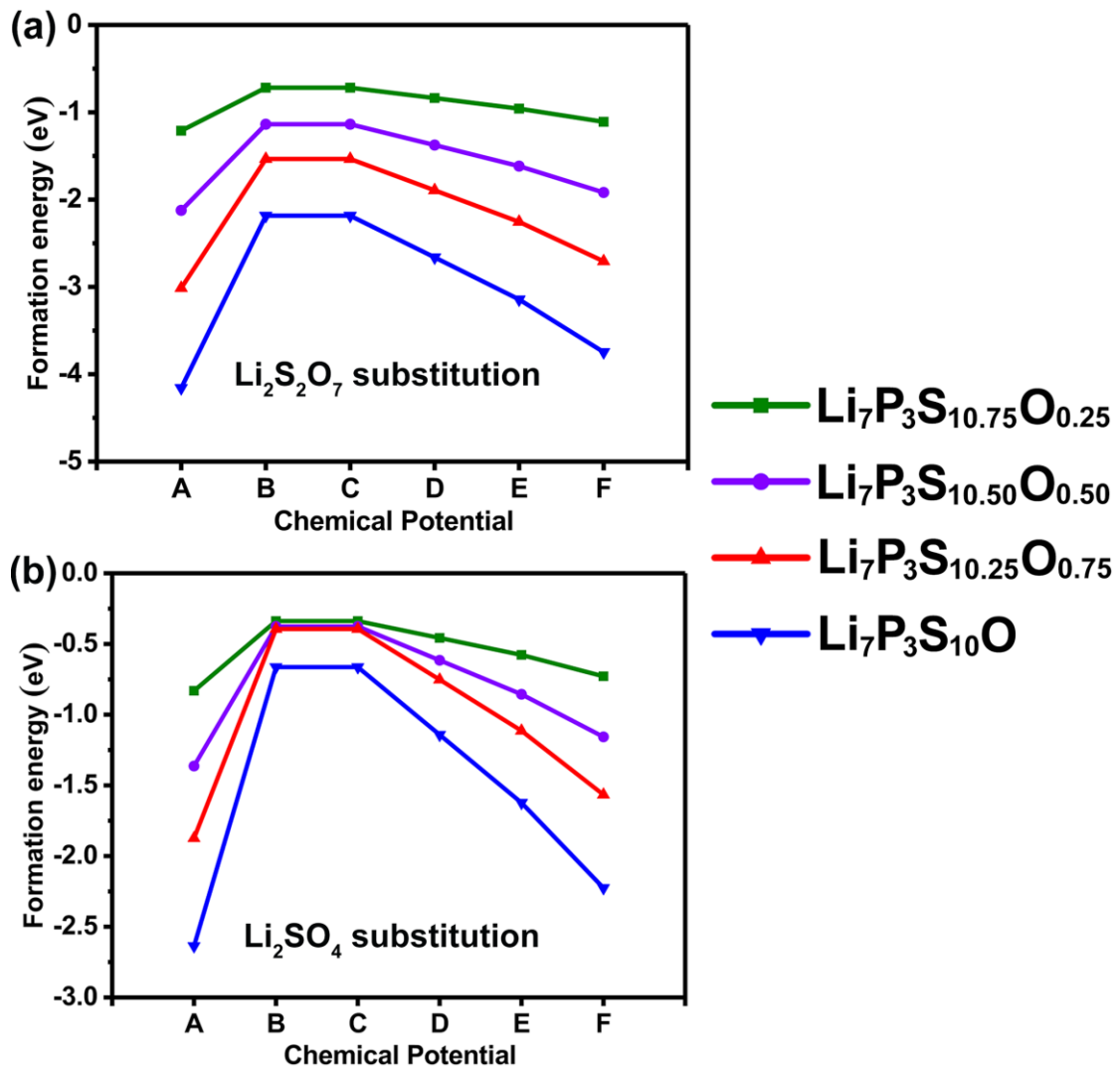


Fig. S19 The calculated formation energies for (a) $Li_2S_2O_7$ substitution and (b) Li_2SO_4 substitution as a function of the chemical potentials at points A-F.

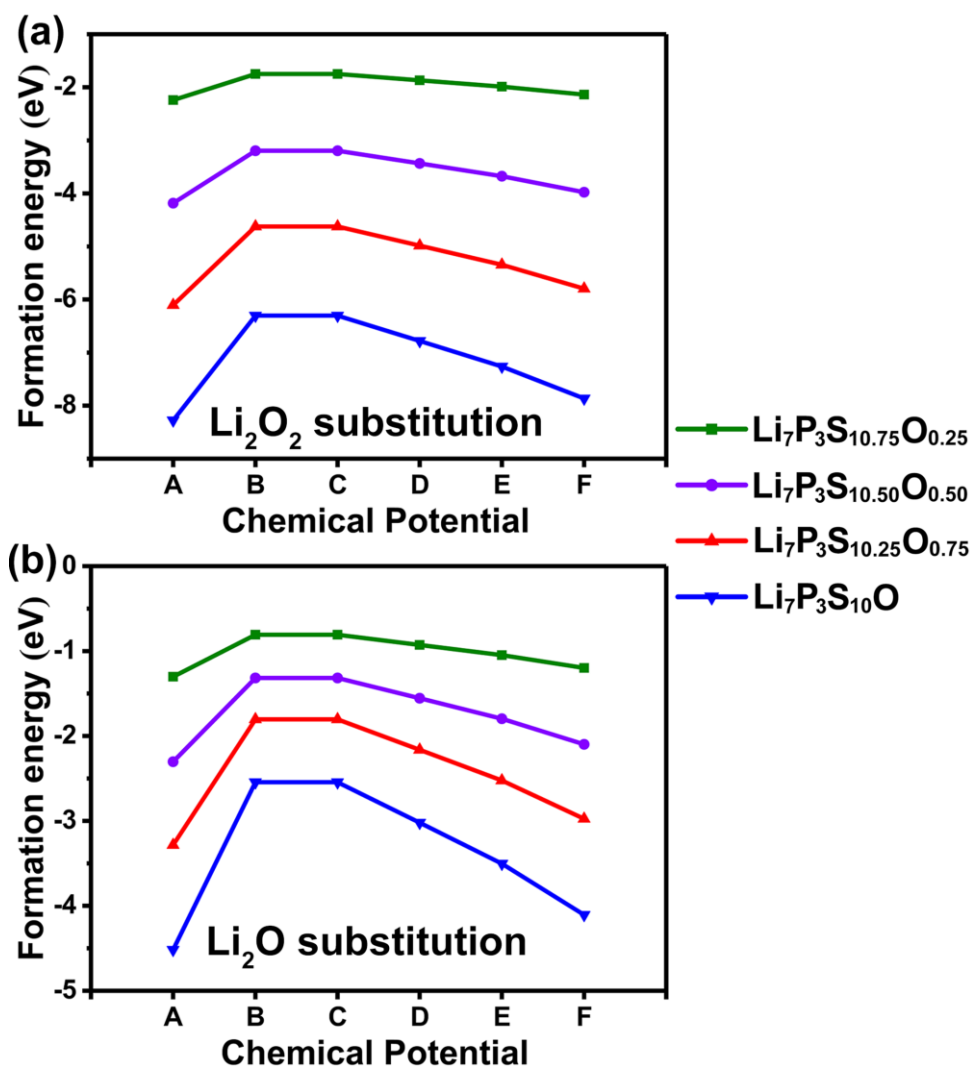


Fig. S20 The calculated formation energies for (a) Li_2O_2 substitution and (b) Li_2O substitution as a function of the chemical potentials at points A-F.

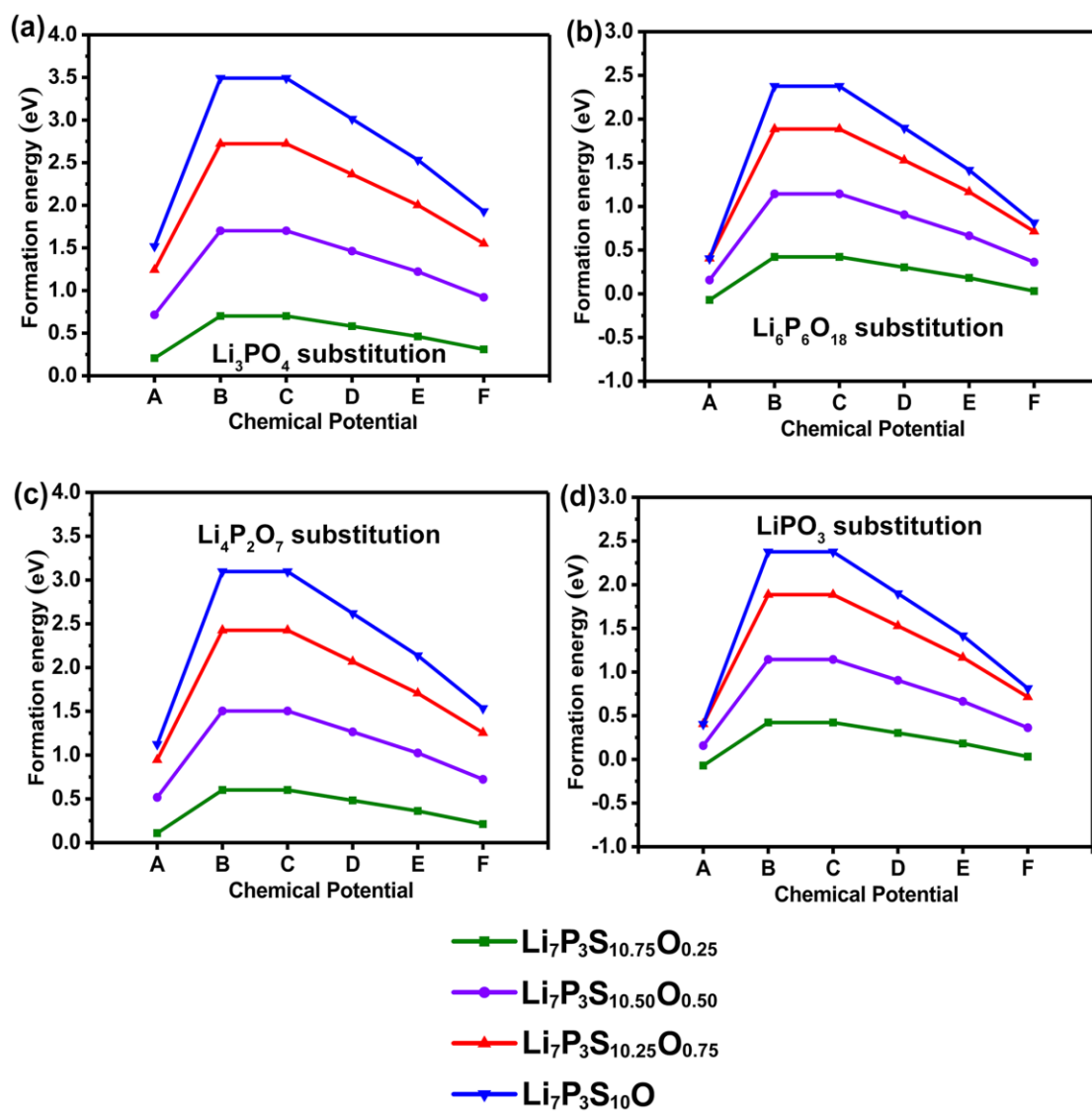


Fig. S21 The calculated formation energies for (a) Li_3PO_4 substitution, (b) $\text{Li}_6\text{P}_6\text{O}_{18}$ substitution (c) $\text{Li}_4\text{P}_2\text{O}_7$ substitution and (d) LiPO_3 substitution as a function of the chemical potentials at points A-F.

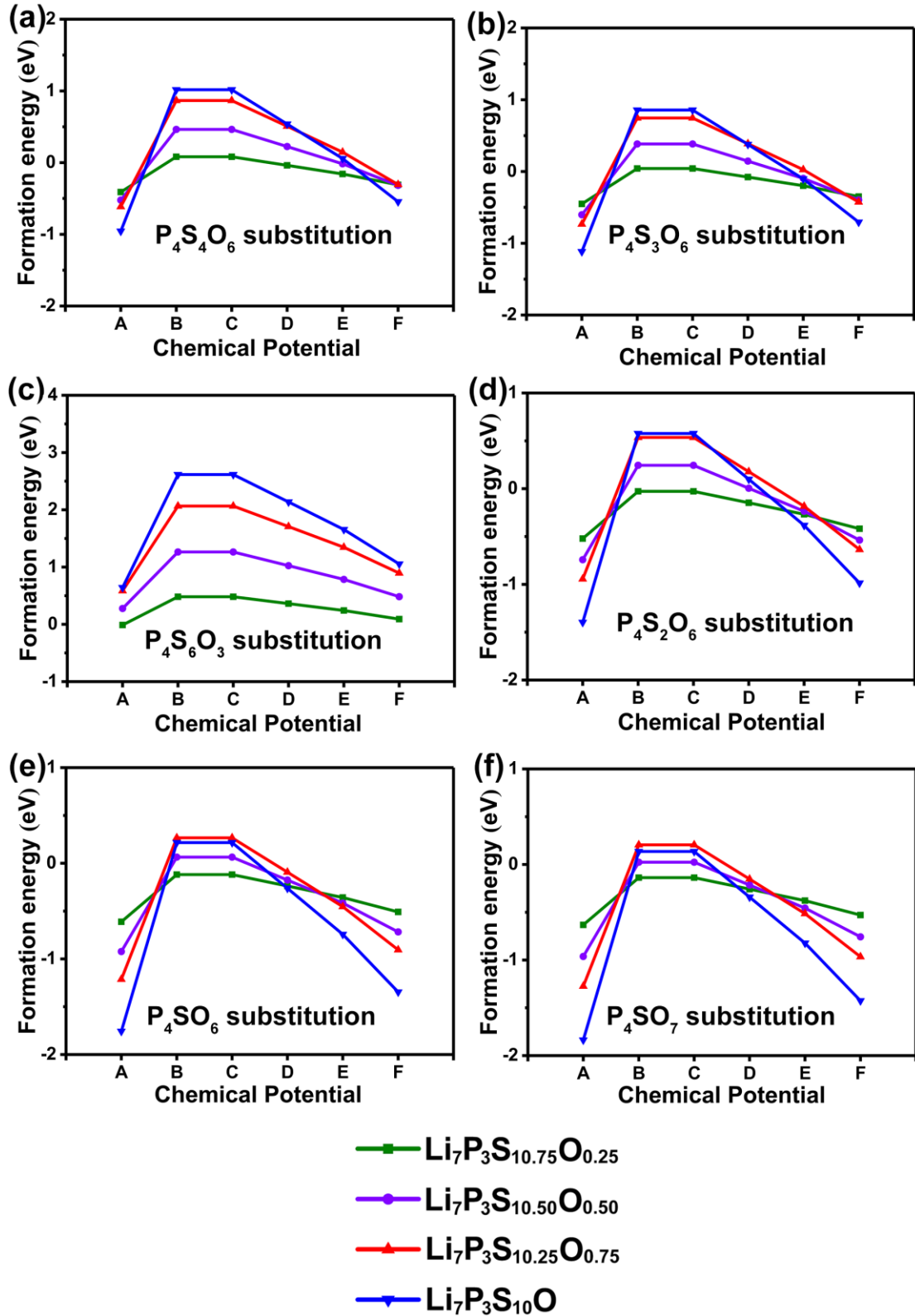


Fig. S22 The calculated formation energies for (a) $P_4S_4O_6$ substitution, (b) $P_4S_3O_6$ substitution, (c) $P_4S_6O_3$ substitution, (d) $P_4S_2O_6$ substitution, (e) P_4SO_6 substitution and (f) P_4SO_7 substitution as a function of the chemical potentials at points A-F.

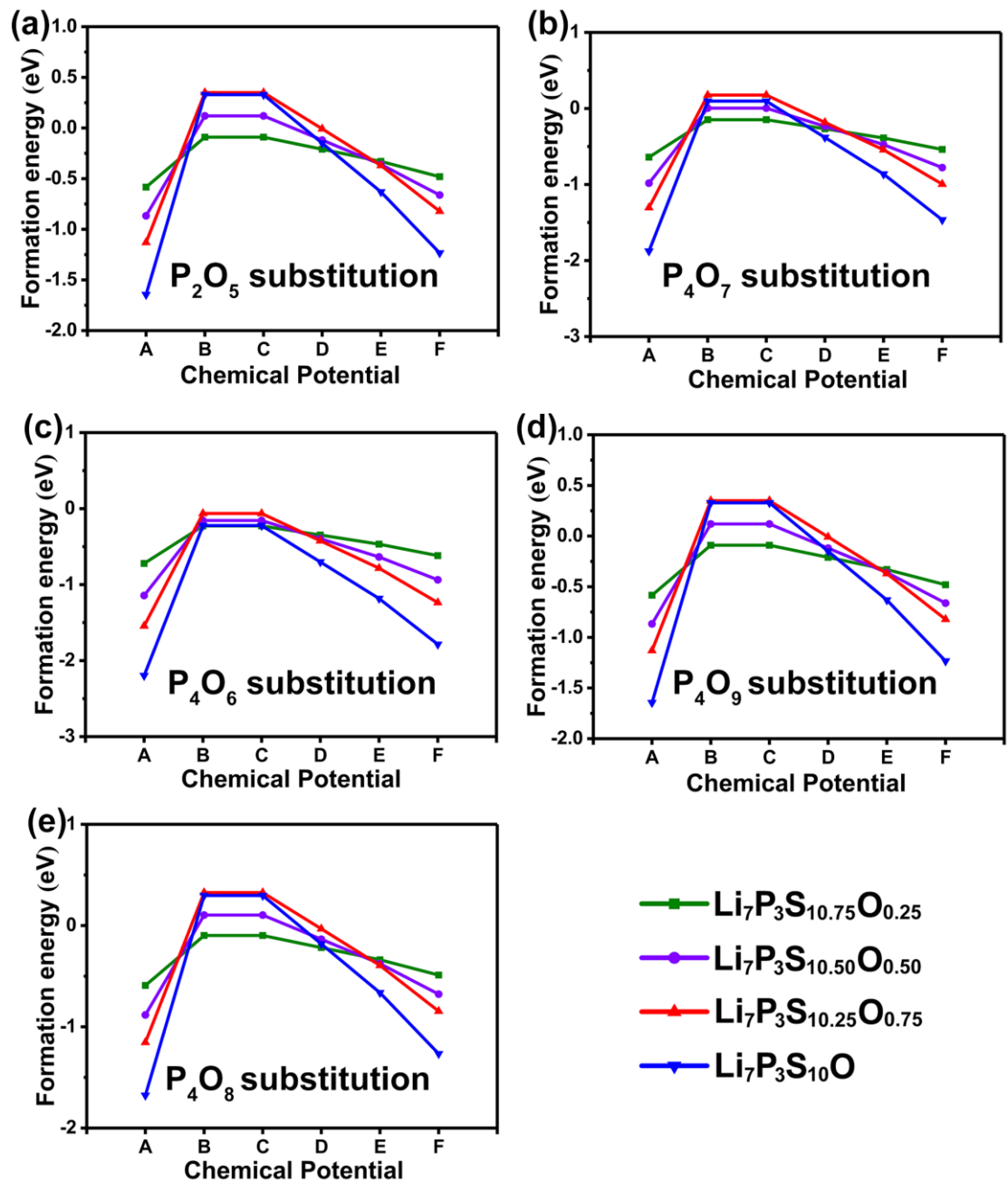


Fig. S23 The calculated formation energies for (a) P_2O_5 substitution, (b) P_4O_7 substitution, (c) P_4O_6 substitution, (d) P_4O_9 substitution and (e) P_4O_8 substitution as a function of the chemical potentials at points A-F.

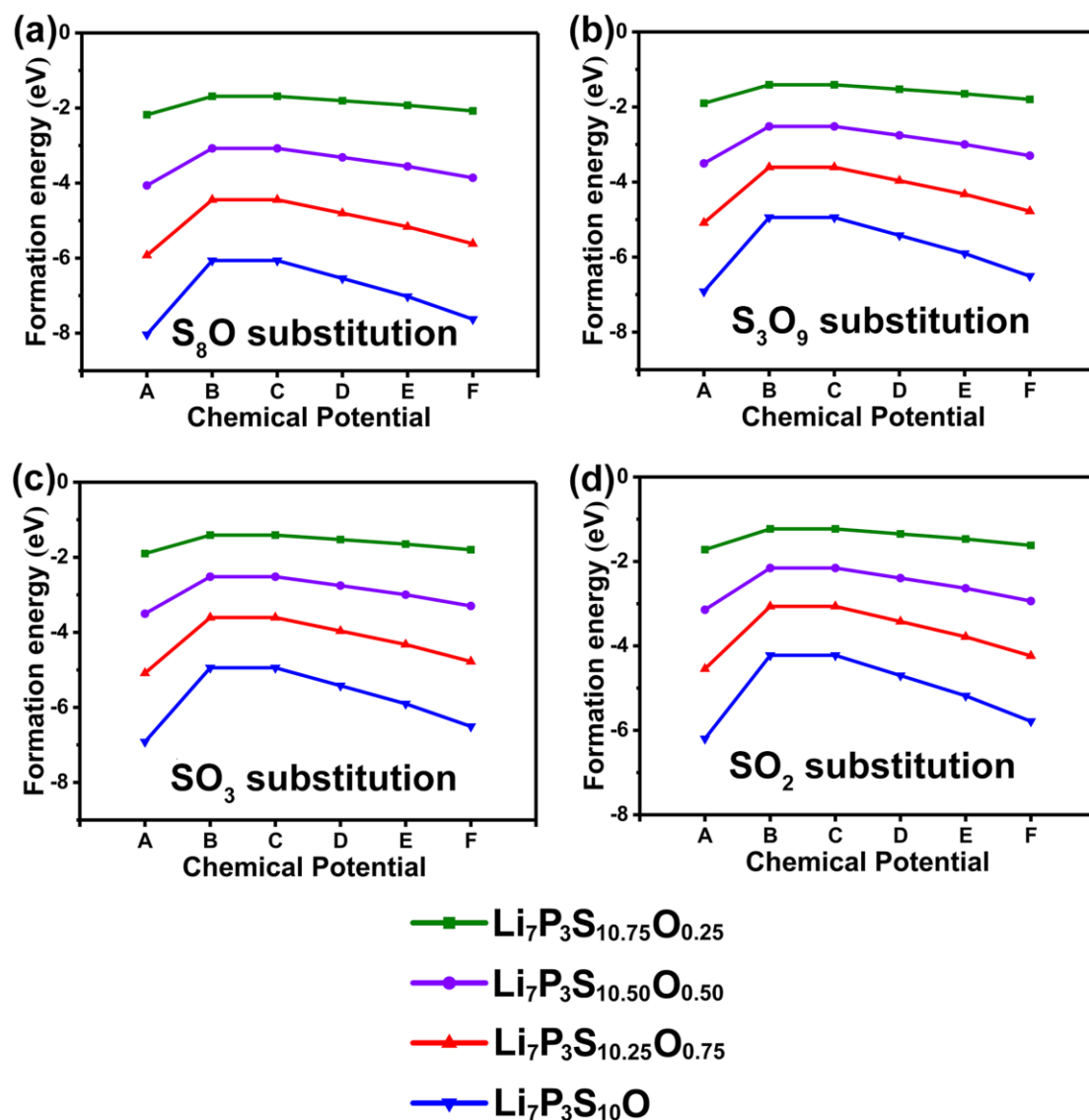


Fig. S24 The calculated formation energies for (a) S_8O substitution, (b) S_3O_9 substitution, (c) SO_3 substitution and (d) SO_2 substitution as a function of the chemical potentials at points A-F.

4. Energy Barriers

Fig. S25 and S26 illustrates Li-ion diffusion pathways and the corresponding energy barriers, respectively. The whole migration process can be divided into two stages: Path① and Path②. As for $\text{Li}_7\text{P}_3\text{S}_{11}$, it is obvious that the energetic barrier of Li-ion diffusion is 0.31 eV, which is close to the reported value.^{3,4} For the case of

Li-ion diffusion in $\text{Li}_7\text{P}_3\text{S}_{11-x}\text{O}_x$ ($x = 0.25, 0.50, 0.75$), the energy barrier of Li-ion diffusion decreases from 0.28 eV to 0.20 eV when oxygen-doping concentration (x) increases from 0.25 to 0.75, indicating oxygen doping plays a key role in the decrease of energetic barrier. On the other hand, for the case of Li-ion diffusion in $\text{Li}_7\text{P}_3\text{S}_{10}\text{O}$, the corresponding energy barrier of Li-ion diffusion turns to 0.27 eV.

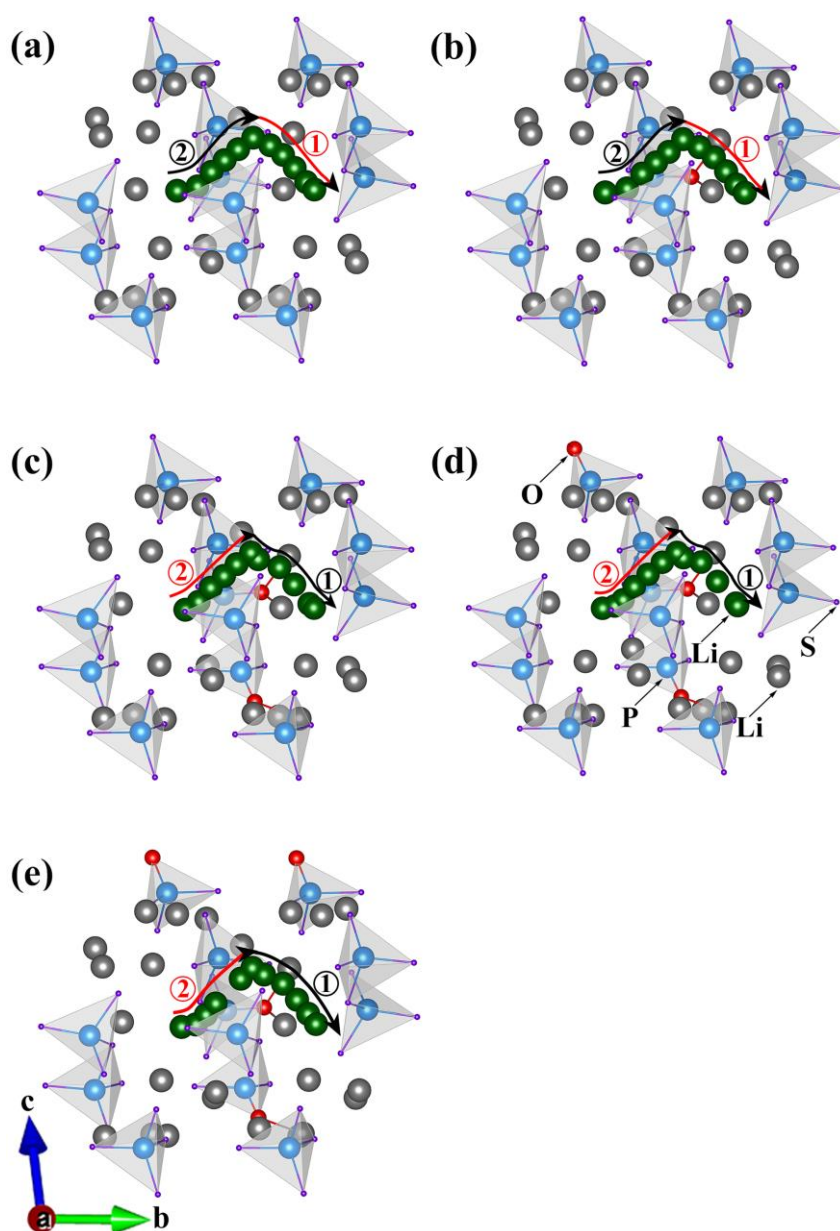


Fig. S25 Li-ion migration pathways for (a) $\text{Li}_7\text{P}_3\text{S}_{11}$, (b) $\text{Li}_7\text{P}_3\text{S}_{10.75}\text{O}_{0.25}$, (c) $\text{Li}_7\text{P}_3\text{S}_{10.50}\text{O}_{0.50}$, (d) $\text{Li}_7\text{P}_3\text{S}_{10.25}\text{O}_{0.75}$ and (e) $\text{Li}_7\text{P}_3\text{S}_{10}\text{O}$, where the green and gray spheres denote diffused Li ion vacancy and non-diffused Li ion separately.

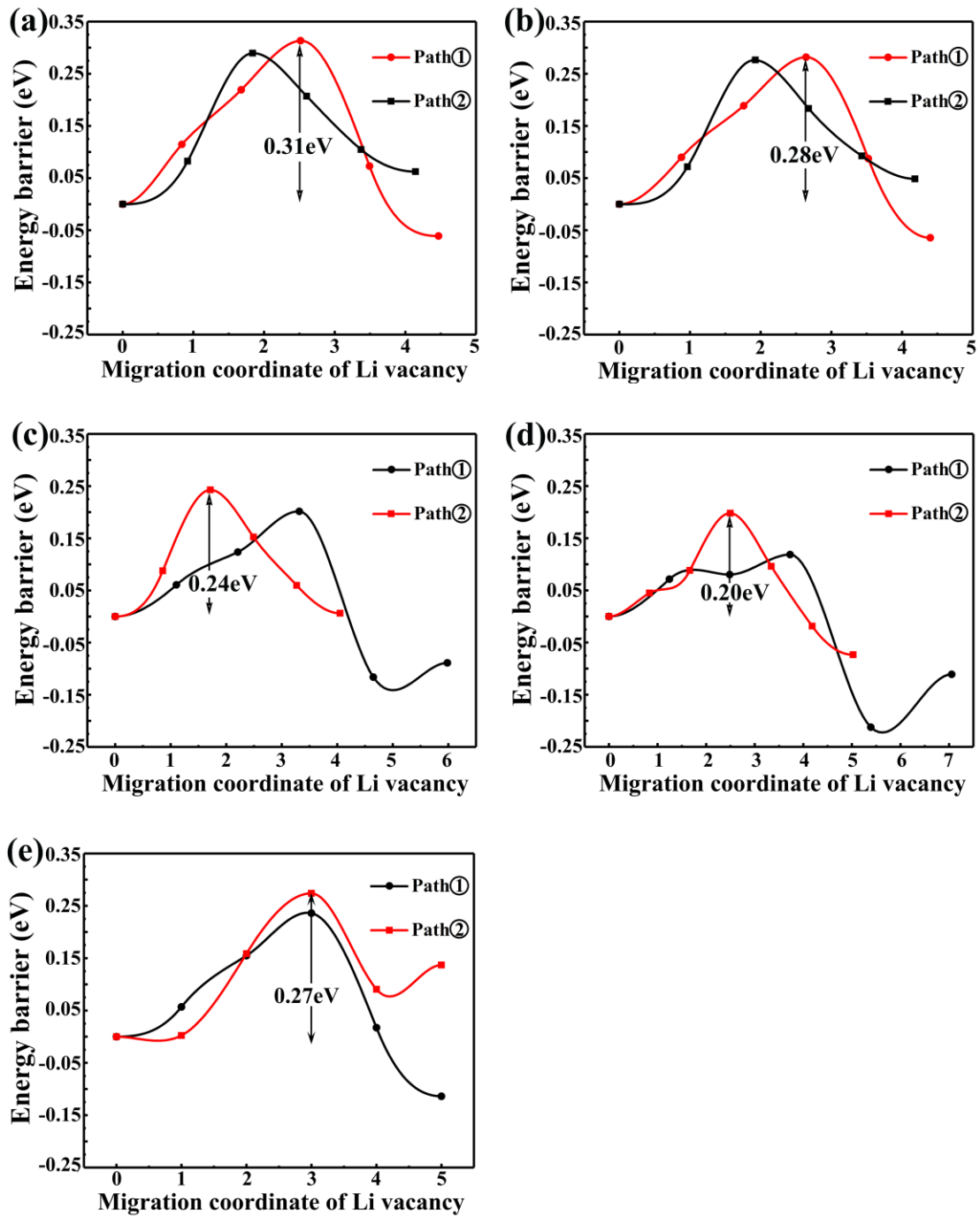


Fig. S26 Calculated energy barriers of Li ions for (a) $\text{Li}_7\text{P}_3\text{S}_{11}$, (b) $\text{Li}_7\text{P}_3\text{S}_{10.75}\text{O}_{0.25}$, (c) $\text{Li}_7\text{P}_3\text{S}_{10.50}\text{O}_{0.50}$, (d) $\text{Li}_7\text{P}_3\text{S}_{10.25}\text{O}_{0.75}$ and (e) $\text{Li}_7\text{P}_3\text{S}_{11}\text{O}$.

Table S4. Energy Barriers of Li-ion Diffusion in $\text{Li}_7\text{P}_3\text{S}_{11-x}\text{O}_x$ ($x = 0.25, 0.50, 0.75$ and 1)

compound	energy barrier (eV)
$\text{Li}_7\text{P}_3\text{S}_{11}$	0.31
$\text{Li}_7\text{P}_3\text{S}_{10.75}\text{O}_{0.25}$	0.28
$\text{Li}_7\text{P}_3\text{S}_{10.50}\text{O}_{0.50}$	0.24
$\text{Li}_7\text{P}_3\text{S}_{10.25}\text{O}_{0.75}$	0.20
$\text{Li}_7\text{P}_3\text{S}_{11}\text{O}$	0.27

The transitional structures with different oxygen-doping concentrations are compared and analyzed. And the structures of $\text{Li}_7\text{P}_3\text{S}_{11}$, $\text{Li}_7\text{P}_3\text{S}_{10.75}\text{O}_{0.25}$, $\text{Li}_7\text{P}_3\text{S}_{10.50}\text{O}_{0.50}$, $\text{Li}_7\text{P}_3\text{S}_{10.25}\text{O}_{0.75}$ and $\text{Li}_7\text{P}_3\text{S}_{11}\text{O}$ at transitional states were presented in Fig. S27. As shown in Fig. S28, it is obvious that there all exist three S atoms interacting with Li atom at transitional states. For $\text{Li}_7\text{P}_3\text{S}_{11}$ and $\text{Li}_7\text{P}_3\text{S}_{10.75}\text{O}_{0.25}$, Li atoms both tend to be located on the triangular edge forming by the interacting sulfur atoms. For $\text{Li}_7\text{P}_3\text{S}_{10.75}\text{O}_{0.25}$, Li-S₁₀ distance is closer to Li-S₁₁ distance relative to those in $\text{Li}_7\text{P}_3\text{S}_{11}$, which makes the weak interaction between Li-S₁₁ and Li-S₁₀ be more balanced. Moreover, Li-S₇ distance is slightly elongated, which induces the smaller energy barrier of Li diffusion in $\text{Li}_7\text{P}_3\text{S}_{10.75}\text{O}_{0.25}$ than that in $\text{Li}_7\text{P}_3\text{S}_{11}$.

For $\text{Li}_7\text{P}_3\text{S}_{10.50}\text{O}_{0.50}$, $\text{Li}_7\text{P}_3\text{S}_{10.25}\text{O}_{0.75}$ and $\text{Li}_7\text{P}_3\text{S}_{11}\text{O}$, Li atoms all tend to be distributed at center within the triangular forming by the interacting sulfur atoms. And Li atom is most close to the center in $\text{Li}_7\text{P}_3\text{S}_{10.25}\text{O}_{0.75}$. As a whole, among $\text{Li}_7\text{P}_3\text{S}_{11}$,

$\text{Li}_7\text{P}_3\text{S}_{10.75}\text{O}_{0.25}$, $\text{Li}_7\text{P}_3\text{S}_{10.50}\text{O}_{0.50}$, $\text{Li}_7\text{P}_3\text{S}_{10.25}\text{O}_{0.75}$ and $\text{Li}_7\text{P}_3\text{S}_{11}\text{O}$, the most balanced structure of Li-S in $\text{Li}_7\text{P}_3\text{S}_{10.25}\text{O}_{0.75}$ at transitional state can be observed, which induces that $\text{Li}_7\text{P}_3\text{S}_{10.25}\text{O}_{0.75}$ has the smallest energy barrier among these five compounds.

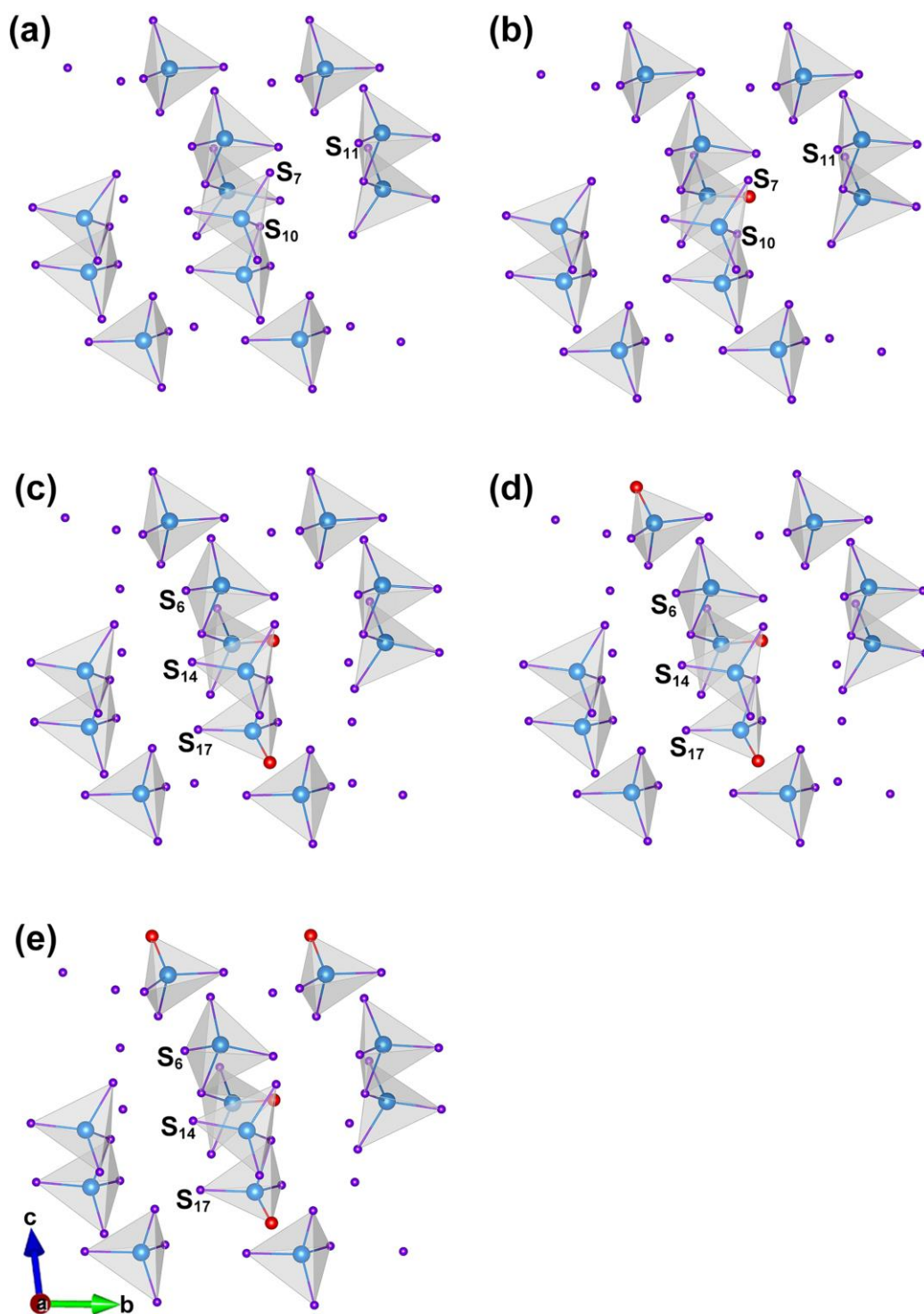


Fig. S27 The local structures of transitional states for (a) $\text{Li}_7\text{P}_3\text{S}_{11}$, (b) $\text{Li}_7\text{P}_3\text{S}_{10.75}\text{O}_{0.25}$, (c) $\text{Li}_7\text{P}_3\text{S}_{10.50}\text{O}_{0.50}$, (d) $\text{Li}_7\text{P}_3\text{S}_{10.25}\text{O}_{0.75}$ and (e) $\text{Li}_7\text{P}_3\text{S}_{11}\text{O}$.

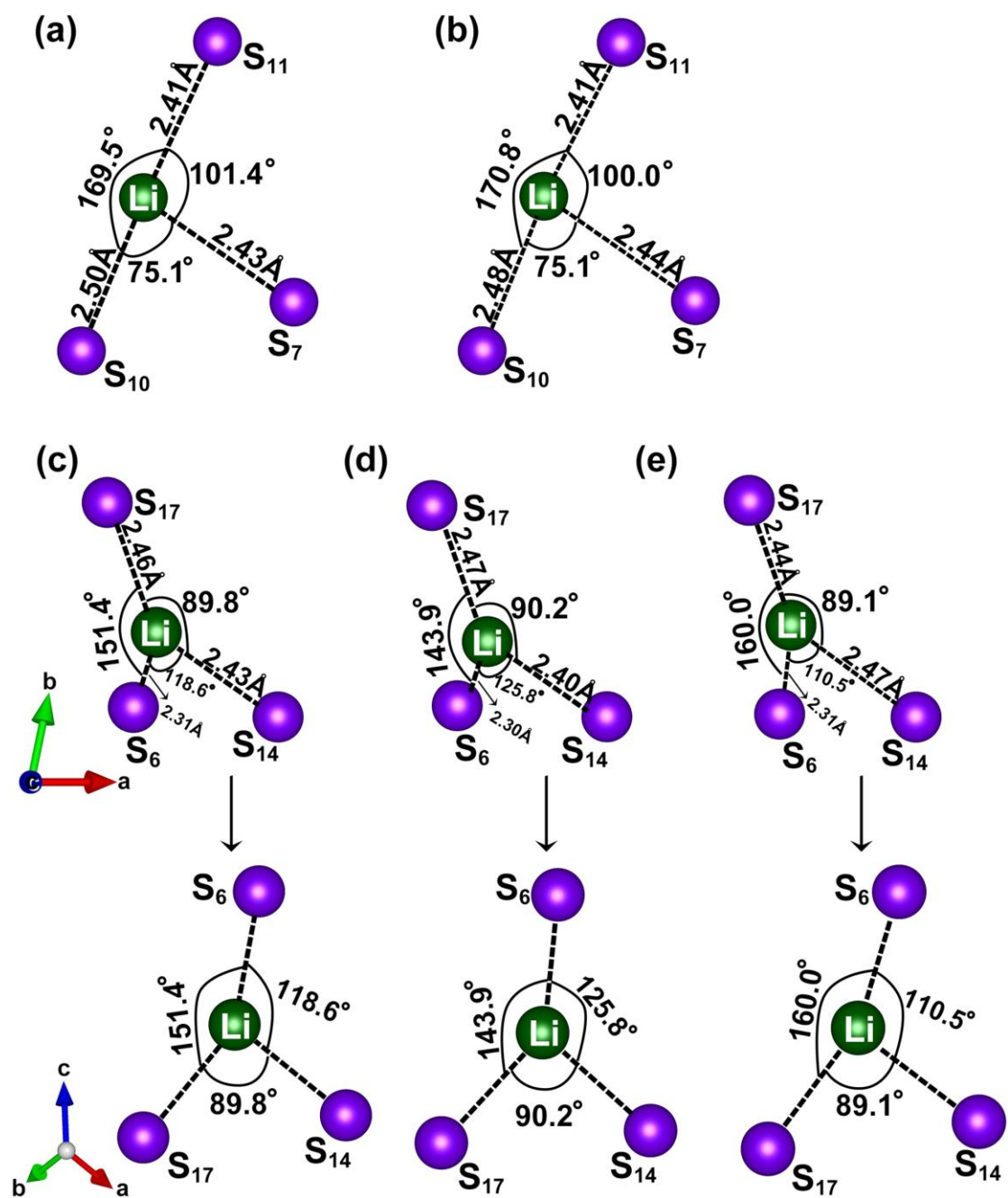


Fig. S28 The local atomic configurations of transitional states for (a) $\text{Li}_7\text{P}_3\text{S}_{11}$, (b) $\text{Li}_7\text{P}_3\text{S}_{10.75}\text{O}_{0.25}$, (c) $\text{Li}_7\text{P}_3\text{S}_{10.50}\text{O}_{0.50}$, (d) $\text{Li}_7\text{P}_3\text{S}_{10.25}\text{O}_{0.75}$ and (e) $\text{Li}_7\text{P}_3\text{S}_{11}\text{O}$.

5. Analysis on the Thermal Stabilities of $\text{Li}_7\text{P}_3\text{S}_{11}$ and $\text{Li}_7\text{P}_3\text{S}_{10.25}\text{O}_{0.75}$

We assessed thermal stabilities of $\text{Li}_7\text{P}_3\text{S}_{11}$ and $\text{Li}_7\text{P}_3\text{S}_{10.25}\text{O}_{0.75}$ by *ab initio* molecular dynamic (AIMD) simulations with the NVT ensemble and a Nose-Hoover

thermostat. Fig. S29 exhibits the potential energies of $\text{Li}_7\text{P}_3\text{S}_{11}$ and $\text{Li}_7\text{P}_3\text{S}_{10.25}\text{O}_{0.75}$ as a function of MD time, respectively. It is confirmed that $\text{Li}_7\text{P}_3\text{S}_{11}$ and $\text{Li}_7\text{P}_3\text{S}_{10.25}\text{O}_{0.75}$ both have excellent thermal stabilities.

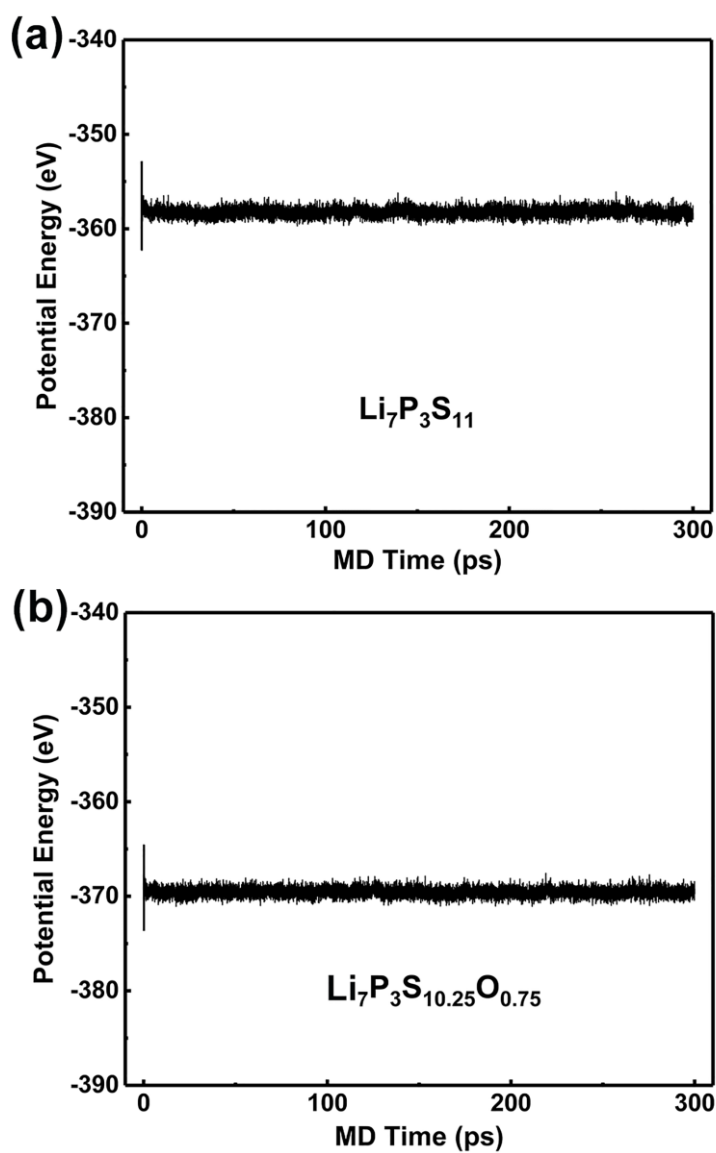


Fig. S29 Total potential energies as a function of MD time for (a) $\text{Li}_7\text{P}_3\text{S}_{11}$ and (b) $\text{Li}_7\text{P}_3\text{S}_{10.25}\text{O}_{0.75}$ at 400 K.

6. Investigation for Migration Process of Li ion

We first considered the direct migration of Li ion between two equivalent sites. As

shown in Fig. S30, the diffusion barrier is about 0.99 eV, which is too high to be consistent with the literature.^{3,4} Therefore, we divided the migration along b direction into two stages.

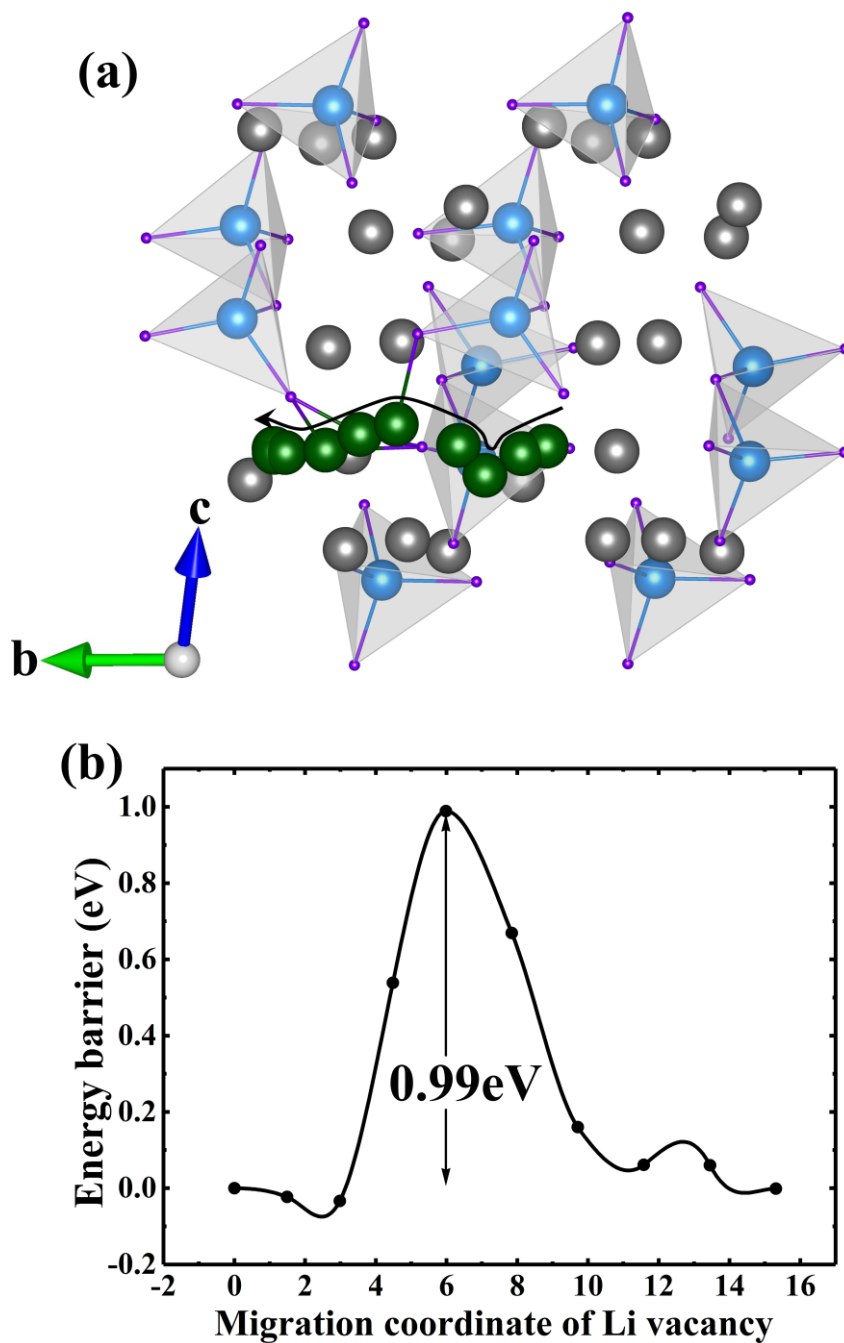


Fig. S30 (a) Schematic of diffusion pathway and (b) the calculated diffusion barrier along b direction.

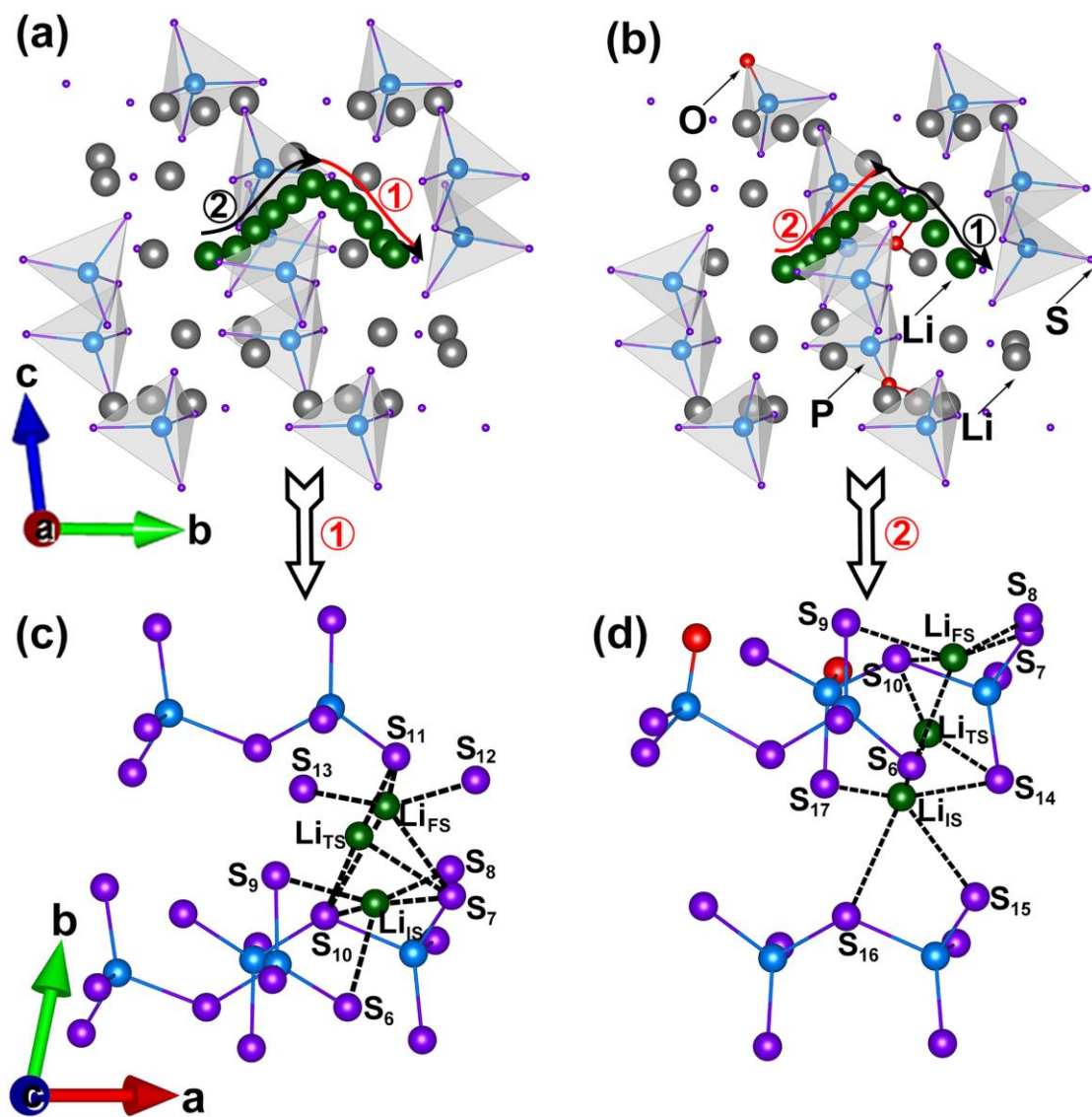


Fig. S31 Li-ion migration pathways for (a) $\text{Li}_7\text{P}_3\text{S}_{11}$ and (b) $\text{Li}_7\text{P}_3\text{S}_{10.25}\text{O}_{0.75}$, together with the local atomic structure around the initial state, transitional state, final state in (c) the path① of $\text{Li}_7\text{P}_3\text{S}_{11}$ and (d) the path② of $\text{Li}_7\text{P}_3\text{S}_{10.25}\text{O}_{0.75}$.

7. *Ab Initio* Molecular Dynamic (AIMD) Simulations

To obtain more accurate and reliable diffusivity of Li-ion in $\text{Li}_7\text{P}_3\text{S}_{11}$ and $\text{Li}_7\text{P}_3\text{S}_{10.25}\text{O}_{0.75}$, *ab initio* molecular dynamic (AIMD) simulations are adopted. As shown in Fig. S32 and S33, the random diffusion of ions in $\text{Li}_7\text{P}_3\text{S}_{11}$ and $\text{Li}_7\text{P}_3\text{S}_{10.25}\text{O}_{0.75}$ can be presented by the mean square displacements.

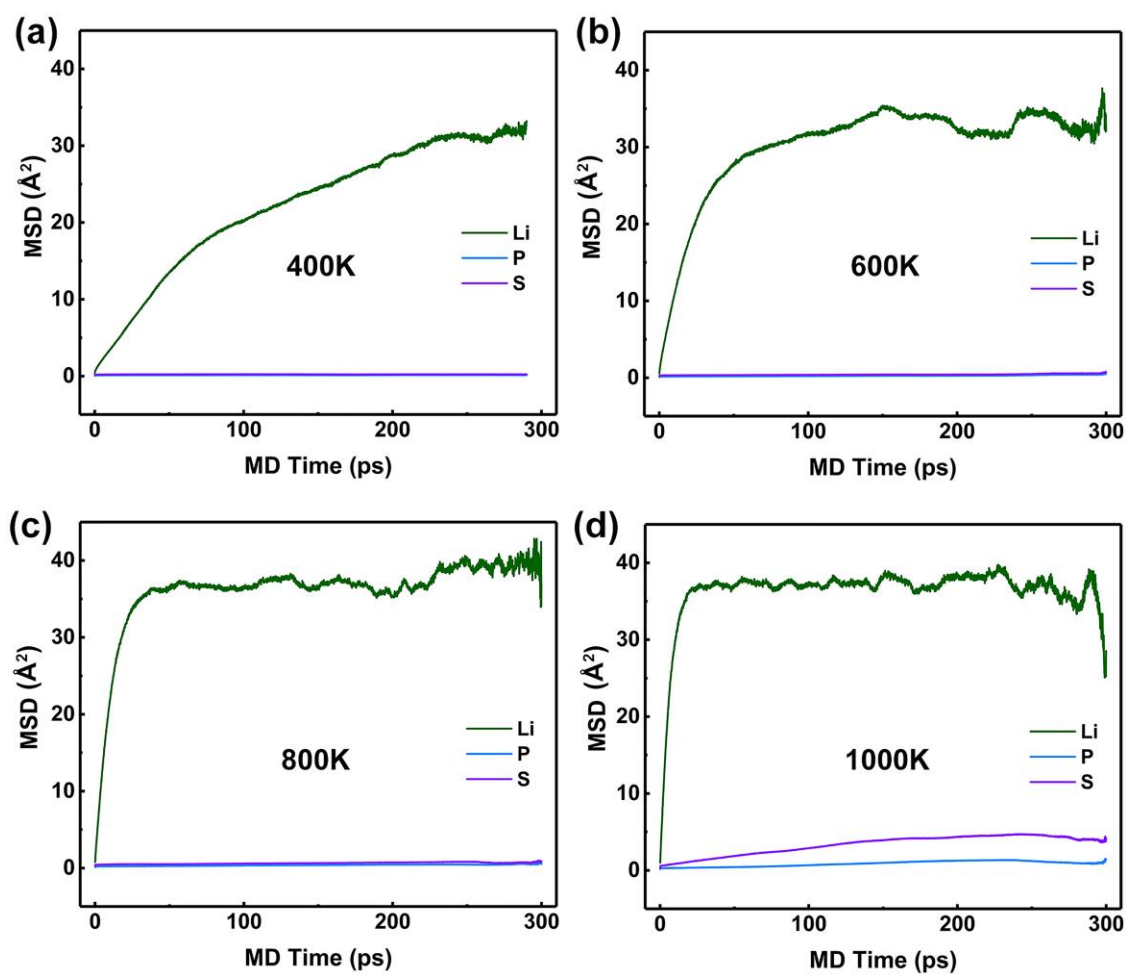


Fig. S32 Mean square displacements for Li, P and S ions in $\text{Li}_7\text{P}_3\text{S}_{11}$ at 400, 600, 800 and 1000 K.

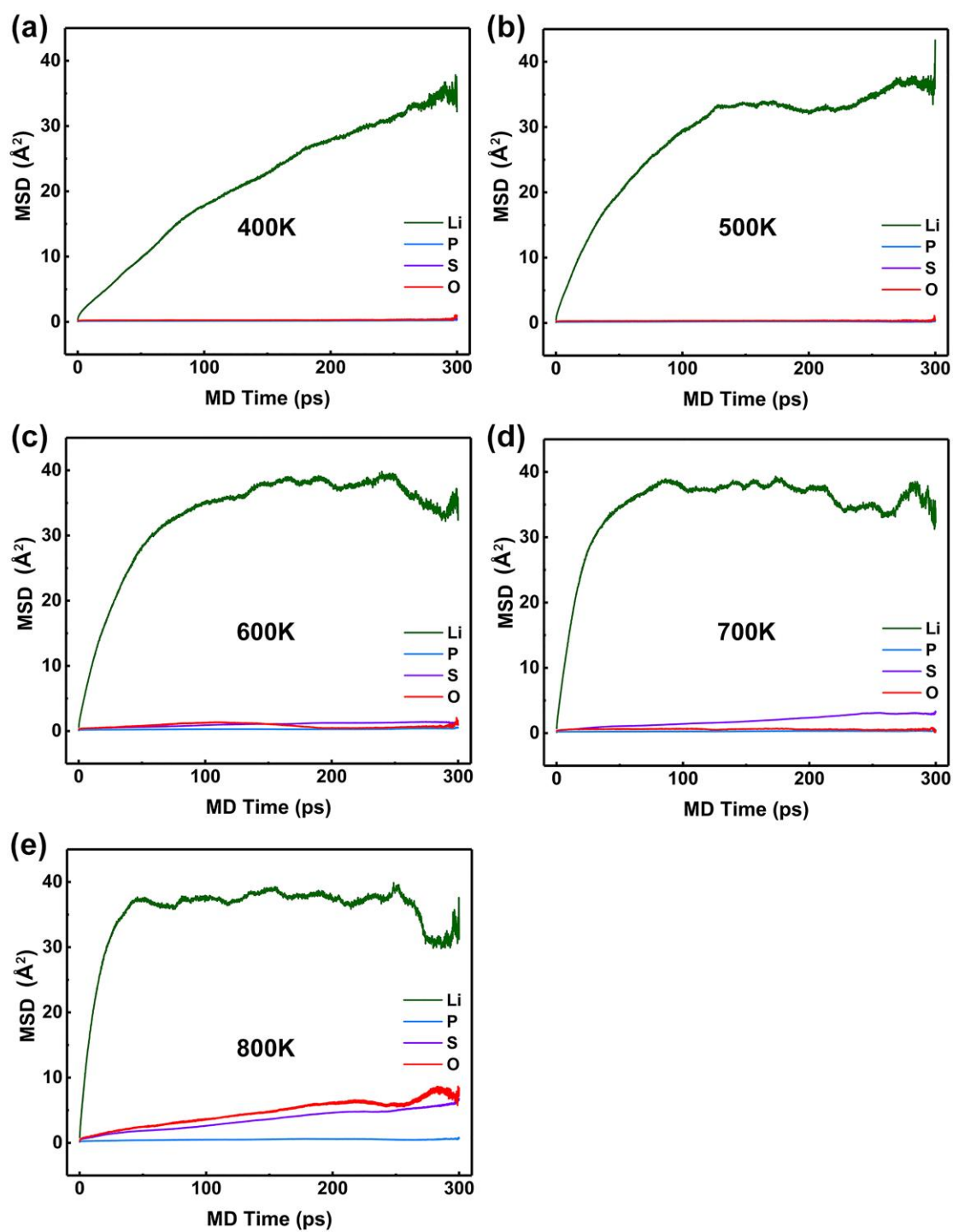


Fig. S33 Mean square displacements for Li, P, S and O ions in $\text{Li}_7\text{P}_3\text{S}_{10.25}\text{O}_{0.75}$ at 400, 500, 600, 700 and 800 K.

8. Methodology

The van Hove correlation function,⁴⁻⁶ split into the self-part G_s and the distinct-part G_d , was used to investigate the correlated Li^+ motions, which can be determined:

$$G_s(r, t) = \frac{1}{4\pi r^2 N_d} \left\langle \sum_{i=1}^{N_d} \delta(r - |\mathbf{r}_i(t_0) - \mathbf{r}_i(t + t_0)|) \right\rangle_{t_0} \quad (1)$$

$$G_d(r, t) = \frac{1}{4\pi r^2 \rho N_d} \left\langle \sum_{i \neq j}^{N_d} \delta(r - |\mathbf{r}_i(t_0) - \mathbf{r}_j(t + t_0)|) \right\rangle_{t_0} \quad (2)$$

where r denotes the radial distance, N_d is the number of diffusing Li ions, $\delta(\dots)$ denotes the one-dimensional Dirac delta function, t_0 is the initial time and $\mathbf{r}_i(t)$ means the diffusion distance for i^{th} ion over the time t . $G_s(r, t)$ is the probability of a ion come to light at a diffusion distance r after time t , whereas $G_d(r, t)$ is the radial distribution of ions at radius r relative to the initial reference ion after time t . Moreover, ρ serves as the “normalization factor” and satisfies $G_d(r, t) = 1$ when $t = 0$.

9. Structural Screening Process for Vacancy Defects

In order to further obtain the effect of Li-vacancy defect on ionic conductivity of $\text{Li}_7\text{P}_3\text{S}_{10.25}\text{O}_{0.75}$, the crystal models of $\text{Li}_{27}\text{P}_{12}\text{S}_{41}\text{O}_3$, $\text{Li}_{26}\text{P}_{12}\text{S}_{41}\text{O}_3$ and $\text{Li}_{25}\text{P}_{12}\text{S}_{41}\text{O}_3$ are constructed, and they correspond to $\text{Li}_{6.75}\text{P}_3\text{S}_{10.25}\text{O}_{0.75}$, $\text{Li}_{6.50}\text{P}_3\text{S}_{10.25}\text{O}_{0.75}$ and $\text{Li}_{6.25}\text{P}_3\text{S}_{10.25}\text{O}_{0.75}$, respectively. Next, we discussed how to search for the most stable crystal structures of $\text{Li}_{6.75}\text{P}_3\text{S}_{10.25}\text{O}_{0.75}$, $\text{Li}_{6.50}\text{P}_3\text{S}_{10.25}\text{O}_{0.75}$ and $\text{Li}_{6.25}\text{P}_3\text{S}_{10.25}\text{O}_{0.75}$, respectively. As shown in Fig. S34, the possible Li-vacancy sites are labeled as numbers (1-28) in the crystal structure of $\text{Li}_7\text{P}_3\text{S}_{10.25}\text{O}_{0.75}$. In order to reduce the

complexity, we search for their most stable crystal structures according to symmetry of structure and total energy.

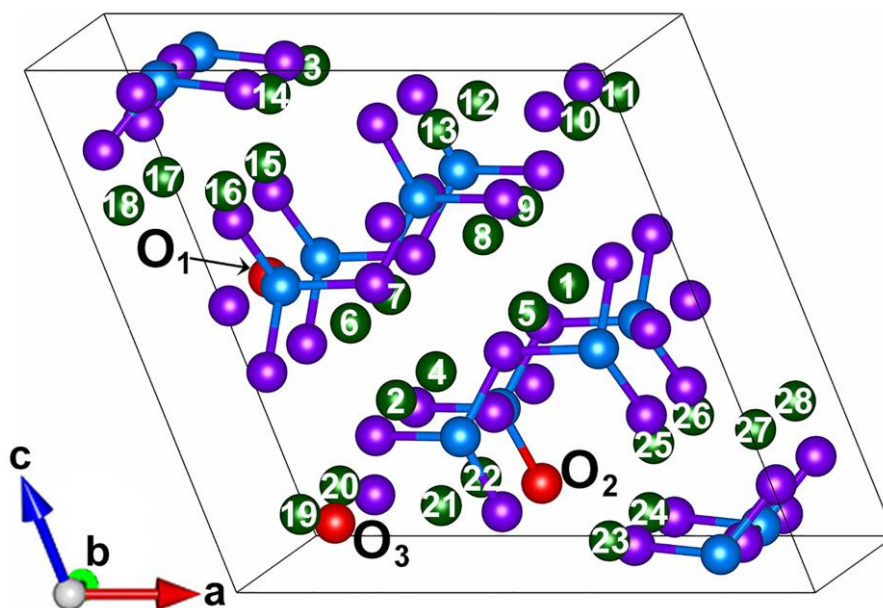


Fig. S34 The crystal structure of $3O_s$ ($Li_7P_3S_{10.25}O_{0.75}$). Here, Li-vacancy sites are labeled as numbers (1-28).

9.1. $Li_{6.75}P_3S_{10.25}O_{0.75}$

For the selection of the first Li-vacancy site in $Li_7P_3S_{10.25}O_{0.75}$, we investigated the relative energies of $Li_{6.75}P_3S_{10.25}O_{0.75}$ as a function of distances between Li vacancy and oxygen (O_1 , O_2 and O_3). Fig. S35-S37 show the possible structures with one Li-vacancy site in $Li_7P_3S_{10.25}O_{0.75}$ and the corresponding relative energies. Interestingly, symmetrical distributions are also found in the plots for the distances and relative energies. And Li vacancy labeled 1 is most likely to occur in $Li_7P_3S_{10.25}O_{0.75}$ due to its smallest energy. As a result, $Li_{6.75}P_3S_{10.25}O_{0.75}$ is formed and presented in Fig. S38.

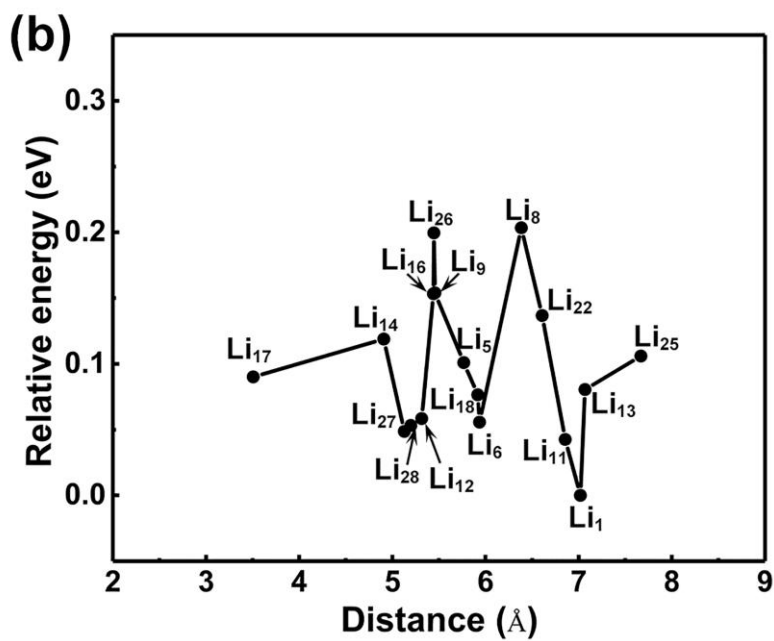
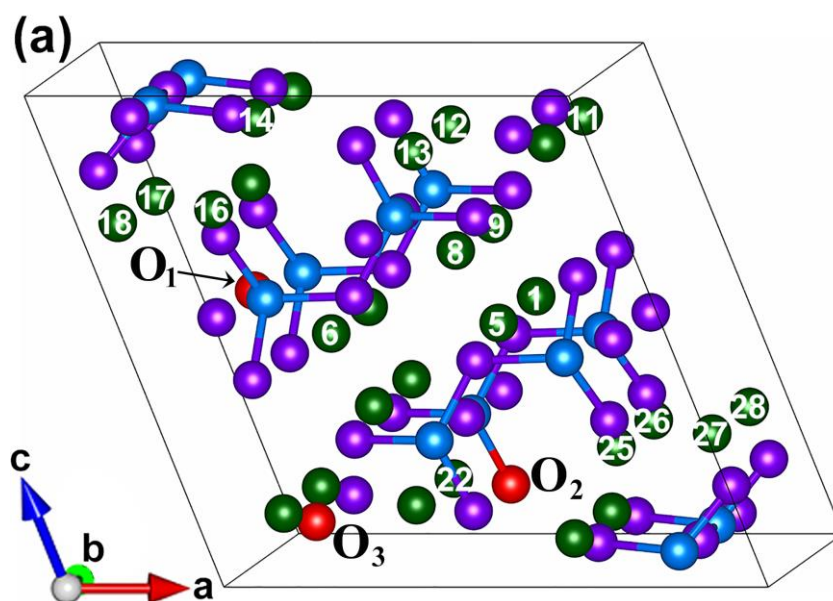


Fig. S35 (a) The crystal structure of $\text{Li}_7\text{P}_3\text{S}_{10.25}\text{O}_{0.75}$. Here, we considered first possible Li-vacancy sites and they were labeled as numbers; (b) The relative energies of $\text{Li}_{6.75}\text{P}_3\text{S}_{10.25}\text{O}_{0.75}$ as a function of the distances between O_1 and possible Li vacancies.

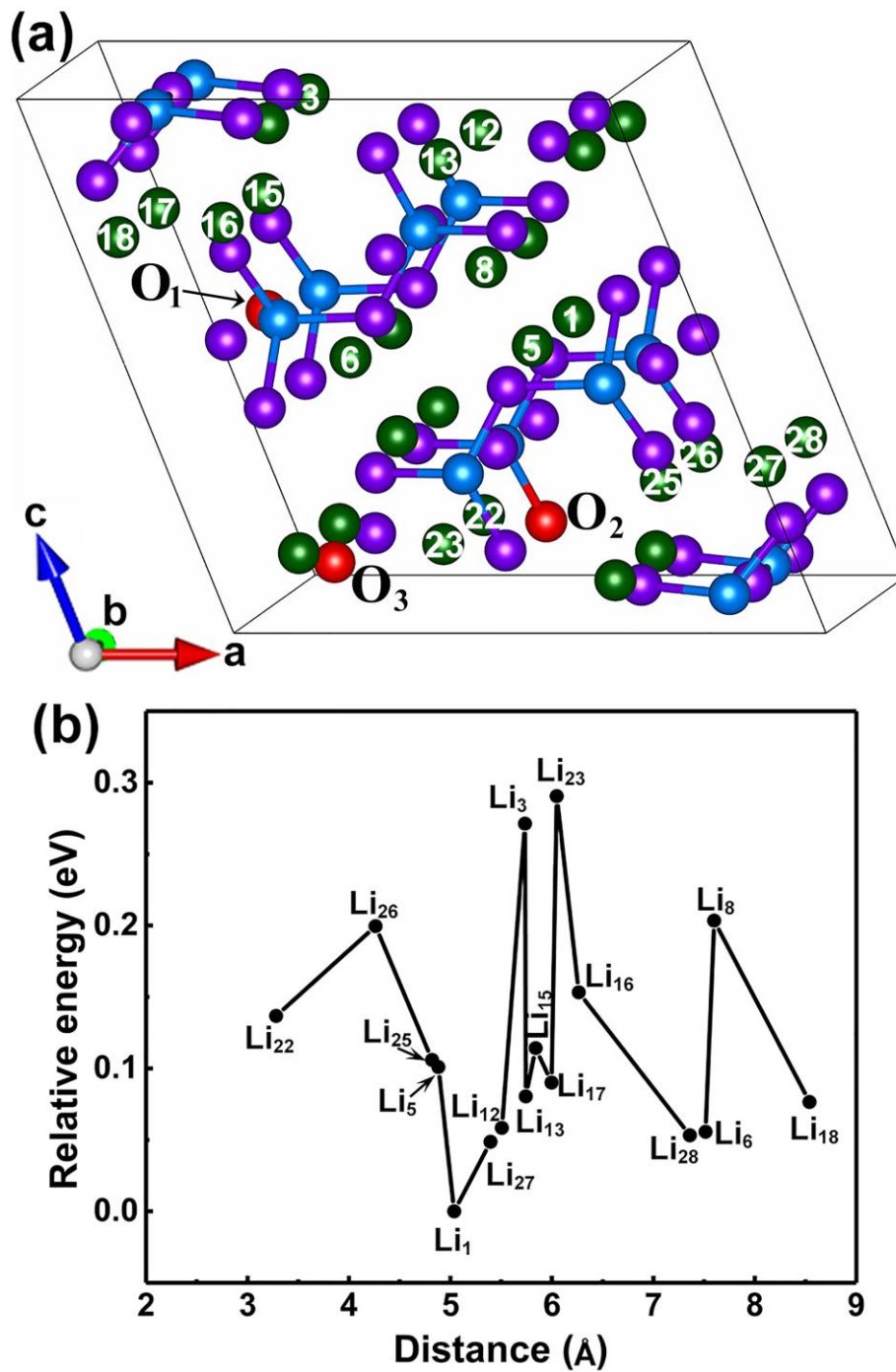


Fig. S36 (a) The crystal structure of $\text{Li}_7\text{P}_3\text{S}_{10.25}\text{O}_{0.75}$. Here, we considered first possible Li-vacancy sites and they were labeled as numbers; (b) The relative energies of $\text{Li}_{6.75}\text{P}_3\text{S}_{10.25}\text{O}_{0.75}$ as a function of the distances between O_2 and possible Li vacancies.

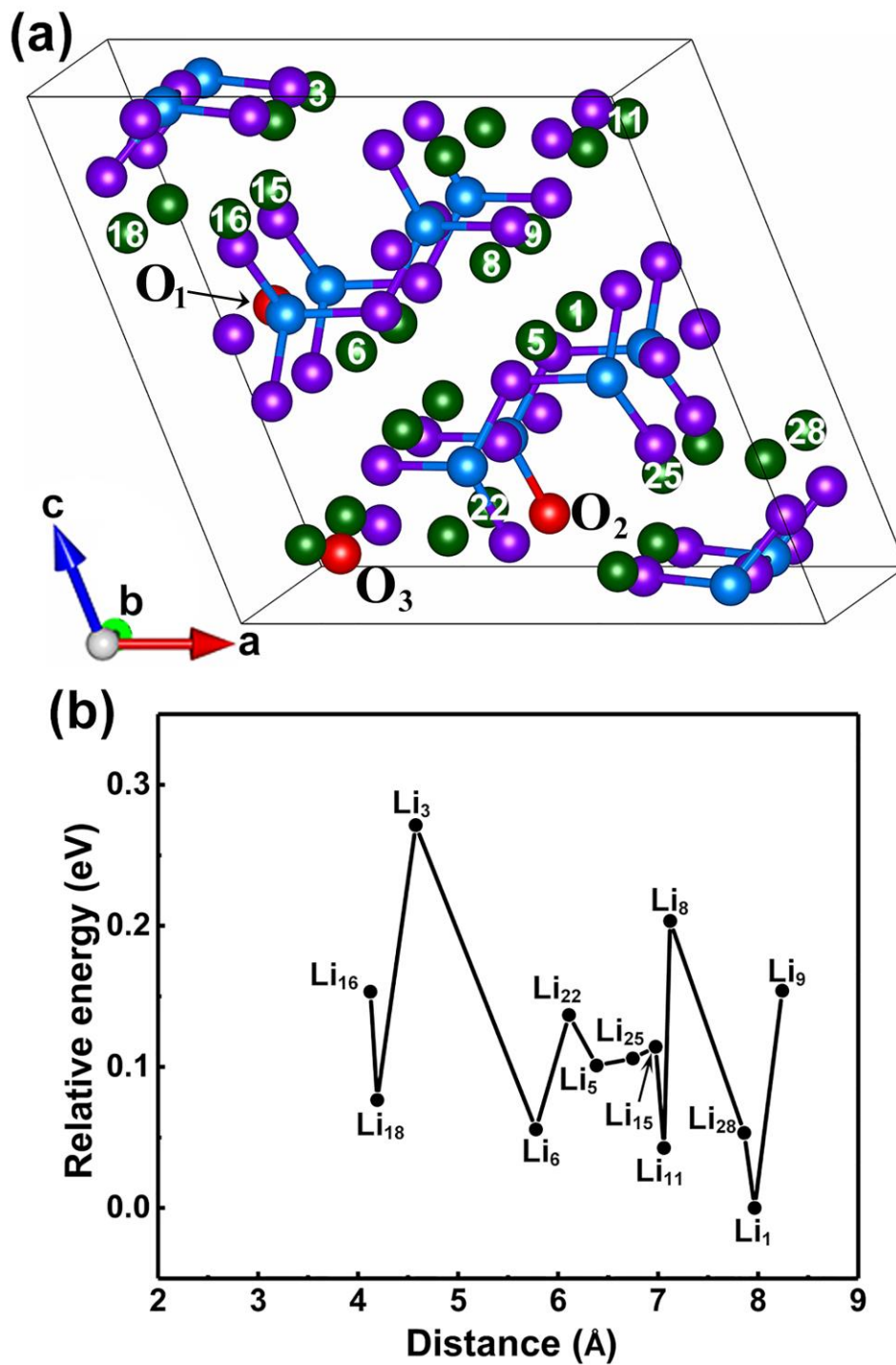


Fig. S37 (a) The crystal structure of $\text{Li}_7\text{P}_3\text{S}_{10.25}\text{O}_{0.75}$. Here, we considered first possible Li-vacancy sites and they were labeled as numbers; (b) The relative energies of $\text{Li}_{6.75}\text{P}_3\text{S}_{10.25}\text{O}_{0.75}$ as a function of the distances between O_3 and possible Li vacancies.

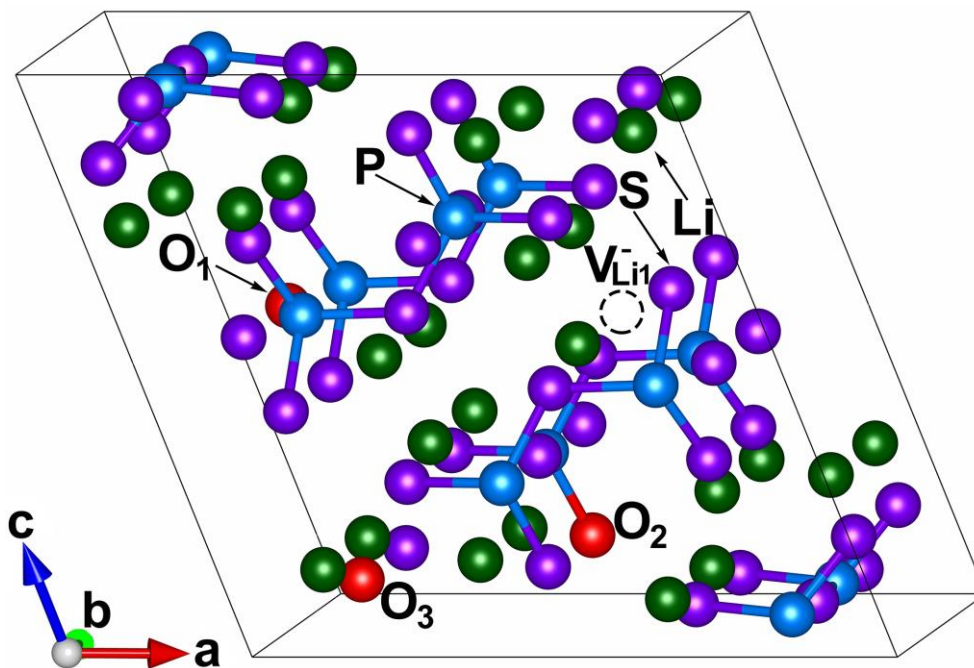


Fig. S38. Ball-and-stick model of $\text{Li}_{6.75}\text{P}_3\text{S}_{10.25}\text{O}_{0.75}$.

9.2. $\text{Li}_{6.50}\text{P}_3\text{S}_{10.25}\text{O}_{0.75}$

Similarly, based on the structure of $\text{Li}_{6.75}\text{P}_3\text{S}_{10.25}\text{O}_{0.75}$, relative energies of $\text{Li}_{6.50}\text{P}_3\text{S}_{10.25}\text{O}_{0.75}$ as a function of distances between the second Li vacancy and oxygen (O_1 , O_2 and O_3) are analyzed and presented in Fig. S39-S42. The symmetrical distributions are also observed. And Li vacancy labeled 2 is most likely to occur in $\text{Li}_{6.75}\text{P}_3\text{S}_{10.25}\text{O}_{0.75}$ due to its smallest energy. As a result, $\text{Li}_{6.50}\text{P}_3\text{S}_{10.25}\text{O}_{0.75}$ is formed and presented in Fig. S43.

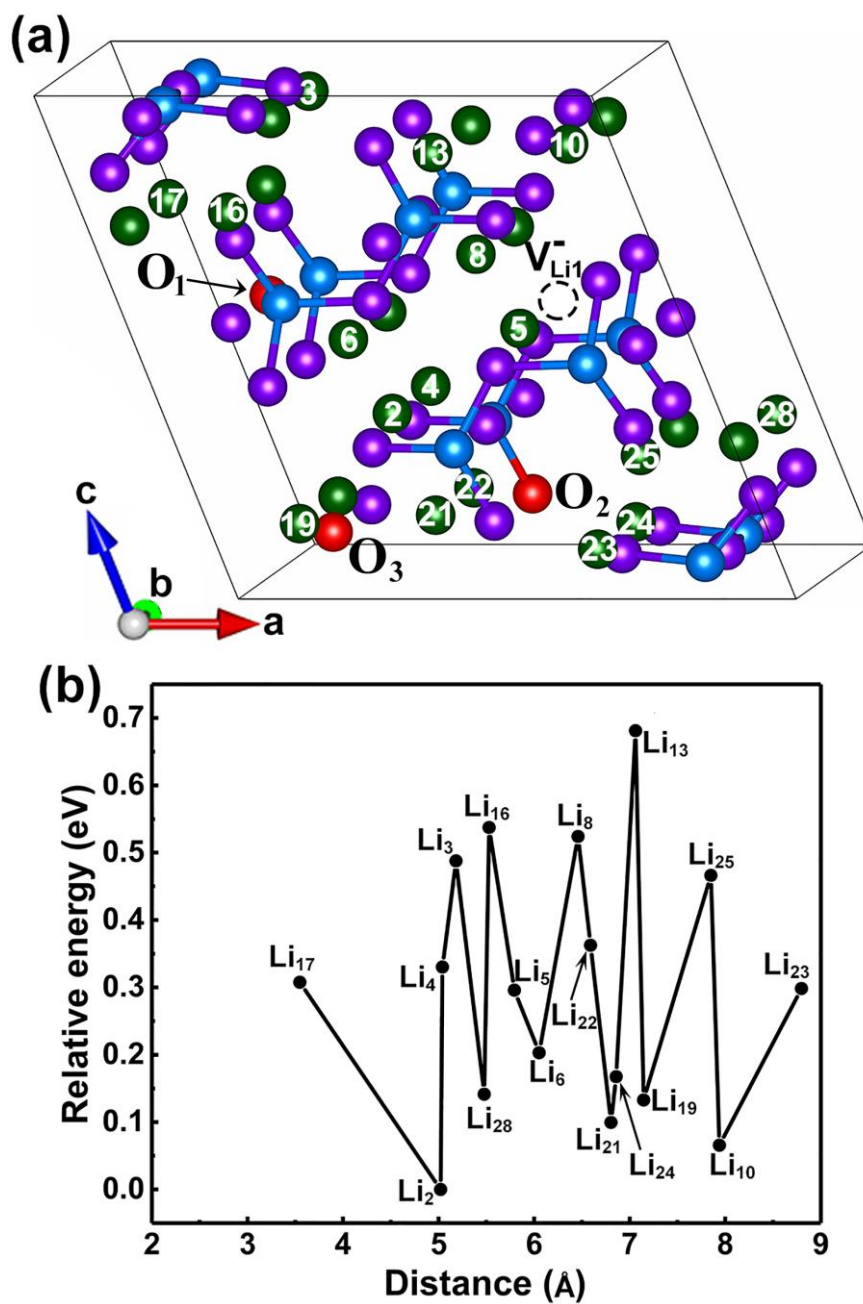


Fig. S39 (a) The crystal structure of $\text{Li}_{6.75}\text{P}_3\text{S}_{10.25}\text{O}_{0.75}$. Here, we considered second possible Li-vacancy sites and they were labeled as numbers; (b) The relative energies of $\text{Li}_{6.50}\text{P}_3\text{S}_{10.25}\text{O}_{0.75}$ as a function of the distances between O_1 and second possible Li vacancies.

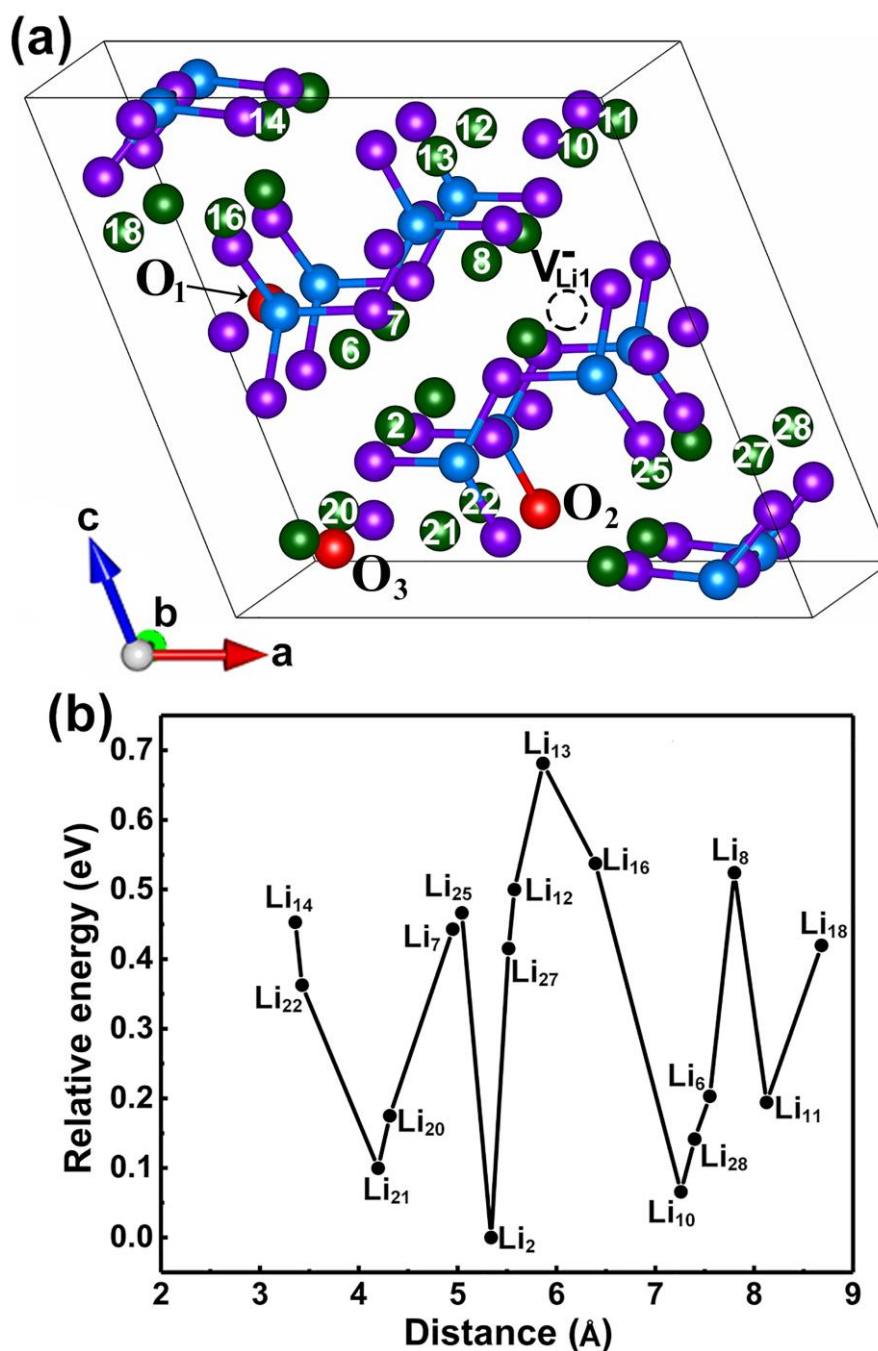


Fig. S40 (a) The crystal structure of $\text{Li}_{6.75}\text{P}_3\text{S}_{10.25}\text{O}_{0.75}$. Here, we considered second possible Li-vacancy sites and they were labeled as numbers; (b) The relative energies of $\text{Li}_{6.50}\text{P}_3\text{S}_{10.25}\text{O}_{0.75}$ as a function of the distances between O_2 and second possible Li vacancies.

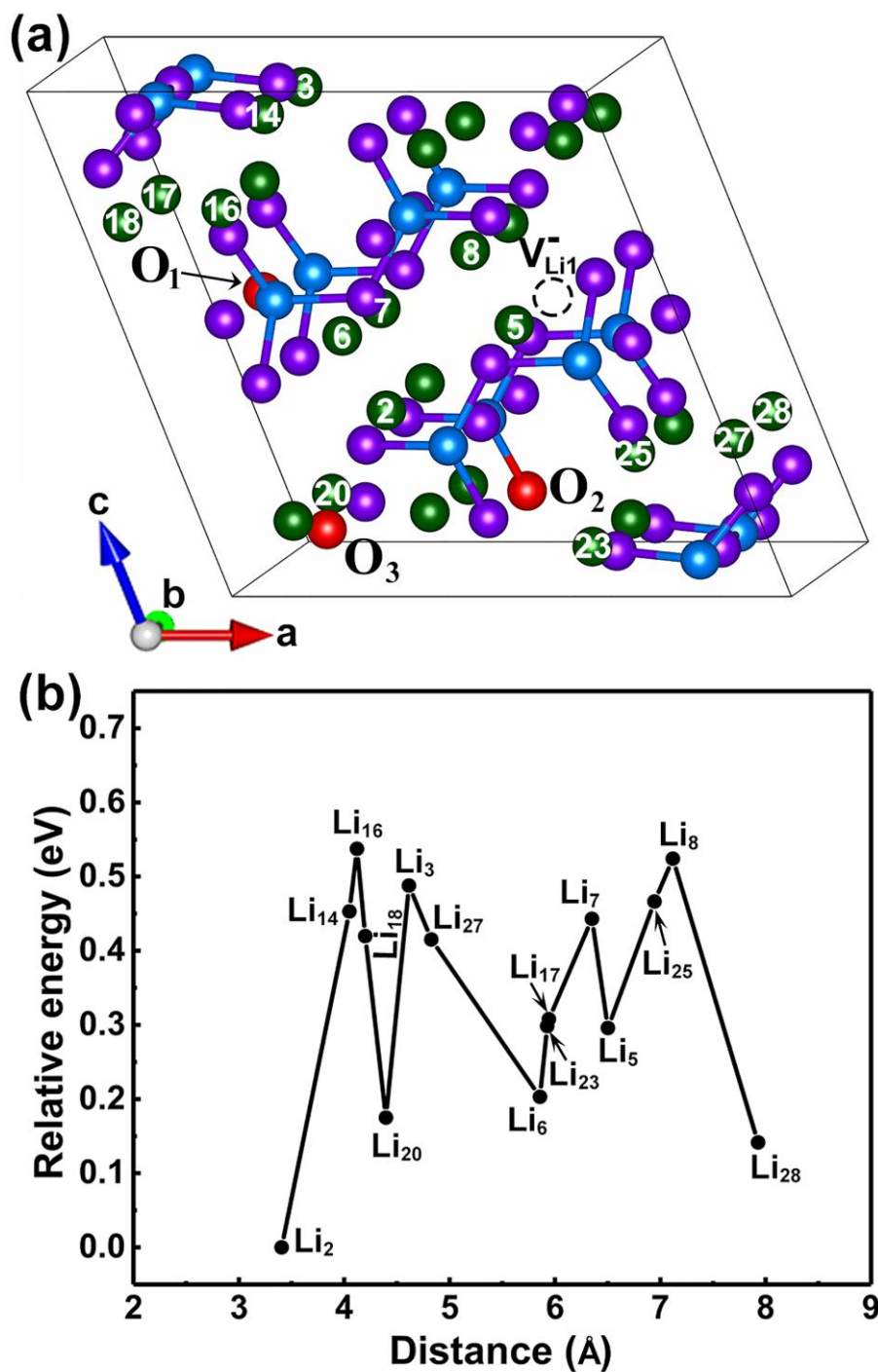


Fig. S41 (a) The crystal structure of $\text{Li}_{6.75}\text{P}_3\text{S}_{10.25}\text{O}_{0.75}$. Here, we considered second possible Li-vacancy sites and they were labeled as numbers; (b) The relative energies of $\text{Li}_{6.50}\text{P}_3\text{S}_{10.25}\text{O}_{0.75}$ as a function of the distances between O_3 and second possible Li vacancies.

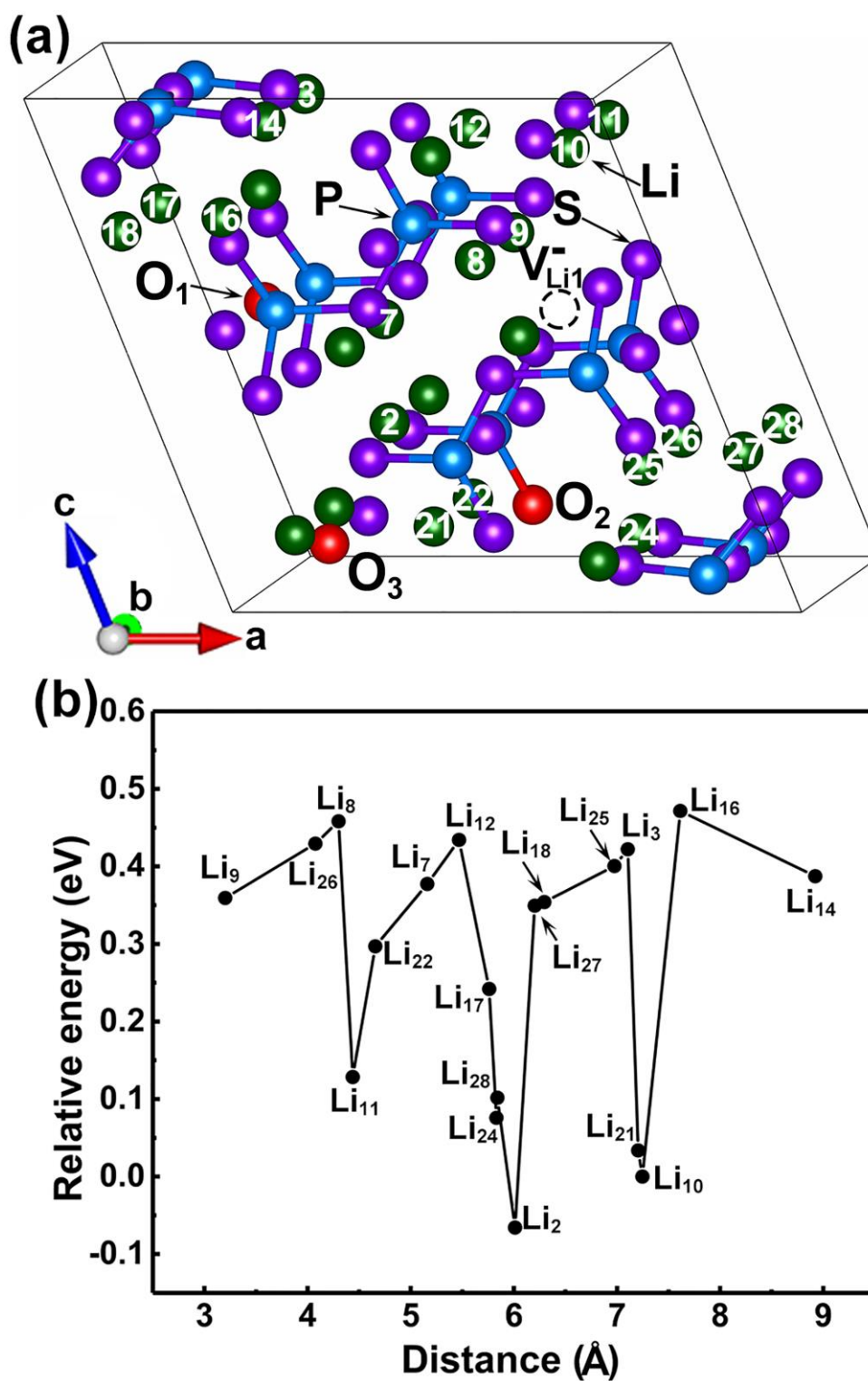


Fig. S42 (a) The crystal structure of $\text{Li}_{6.75}\text{P}_3\text{S}_{10.25}\text{O}_{0.75}$. Here, we considered second possible Li-vacancy sites and they were labeled as numbers; (b) The relative energies of $\text{Li}_{6.50}\text{P}_3\text{S}_{10.25}\text{O}_{0.75}$ as a function of the distances between second possible Li vacancies and V_{Li1}^- .

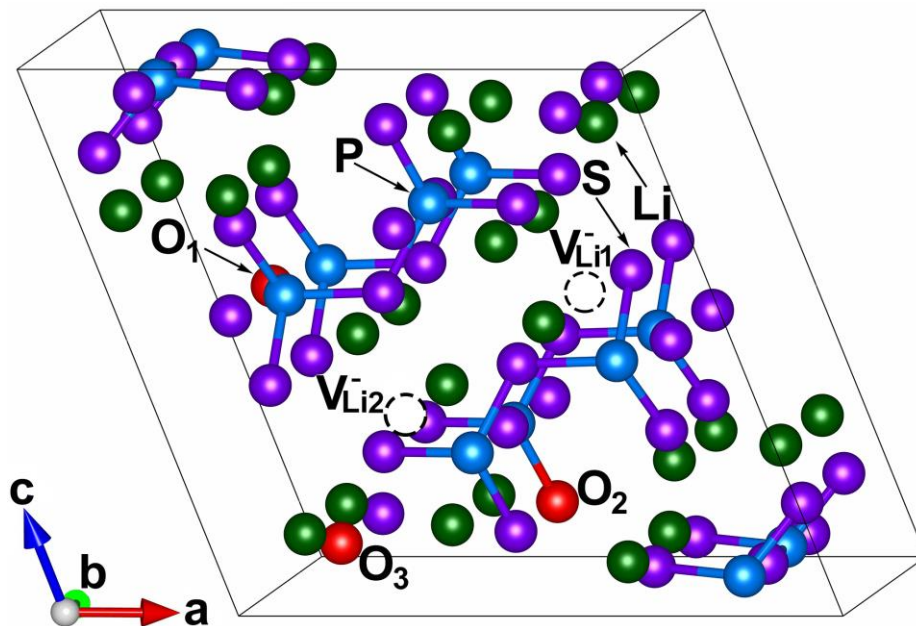


Fig. S43 Ball-and-stick model of $\text{Li}_{6.50}\text{P}_3\text{S}_{10.25}\text{O}_{0.75}$.

9.3. $\text{Li}_{6.25}\text{P}_3\text{S}_{10.25}\text{O}_{0.75}$

Finally, based on the structure of $\text{Li}_{6.50}\text{P}_3\text{S}_{10.25}\text{O}_{0.75}$, Li vacancy labeled 3 is most likely to occur in $\text{Li}_{6.50}\text{P}_3\text{S}_{10.25}\text{O}_{0.75}$ due to its smallest energy (see Fig. S44-S48). And symmetrical distributions between relative energies and the distances are also observed. As a result, $\text{Li}_{6.25}\text{P}_3\text{S}_{10.25}\text{O}_{0.75}$ is formed and presented in Fig. S49.

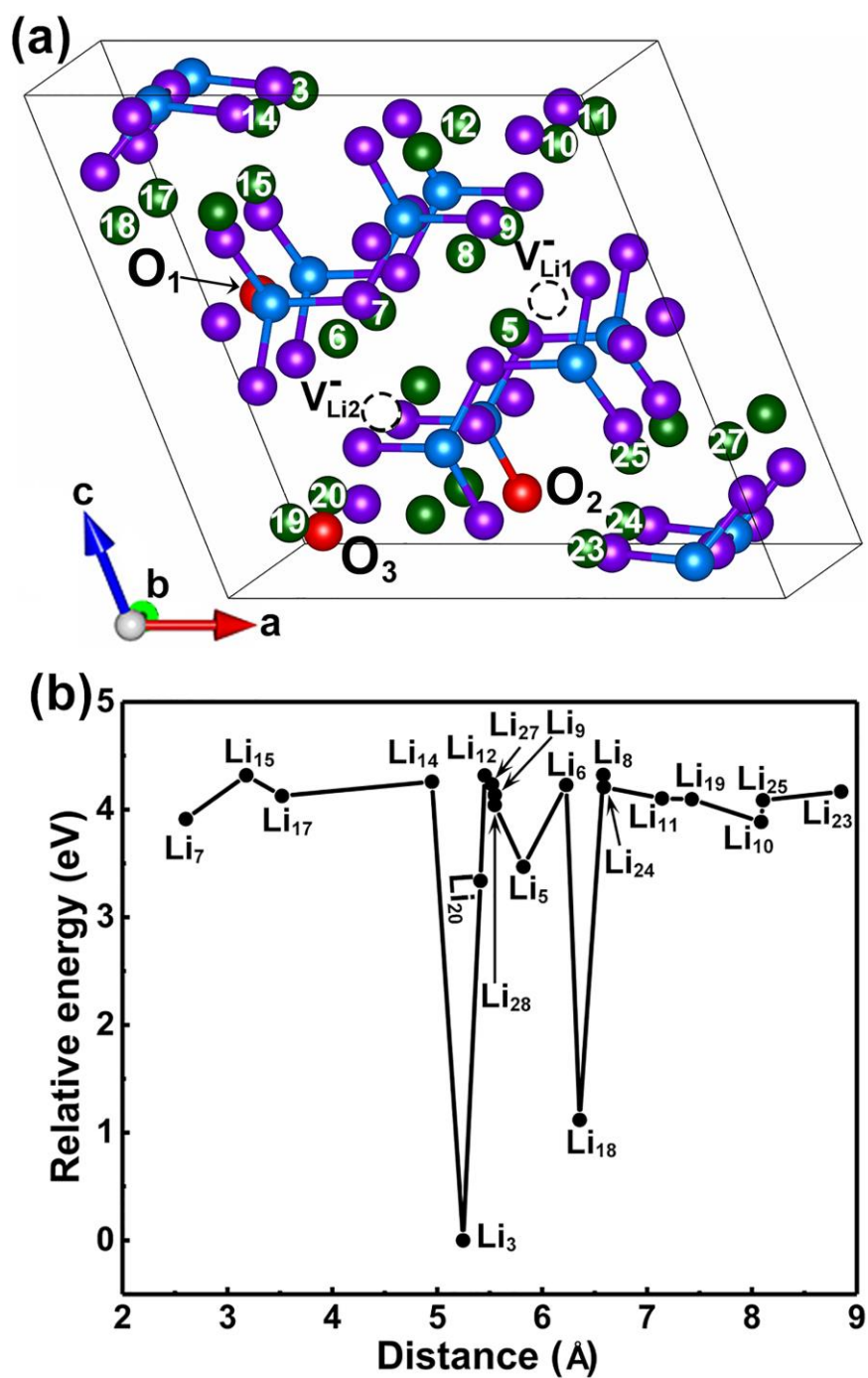


Fig. S44 (a) The crystal structure of $\text{Li}_{6.50}\text{P}_3\text{S}_{10.25}\text{O}_{0.75}$. Here, we considered third possible Li-vacancy sites and they were labeled as numbers; (b) The relative energies of $\text{Li}_{6.25}\text{P}_3\text{S}_{10.25}\text{O}_{0.75}$ as a function of the distances between O_1 and third possible Li vacancies.

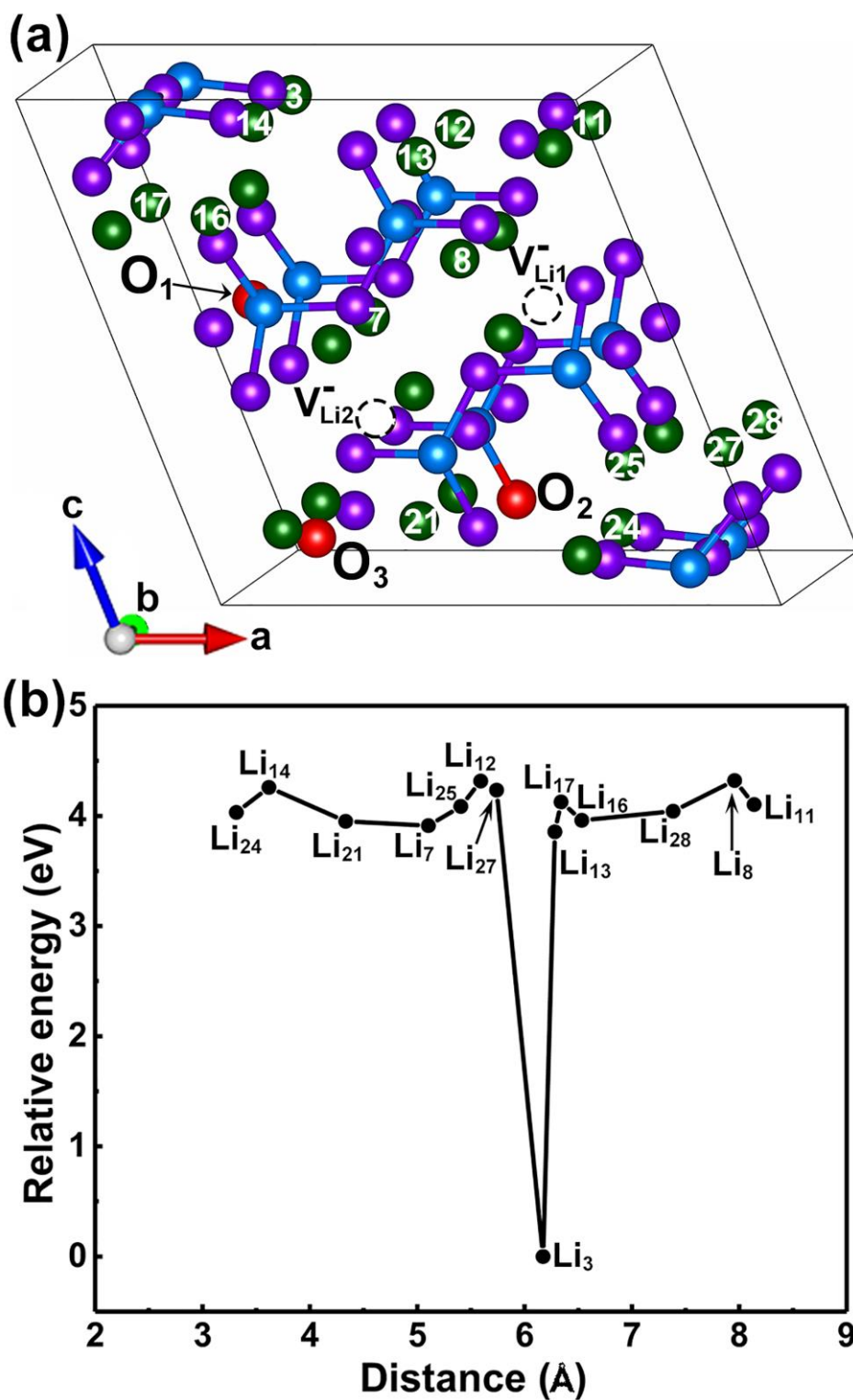


Fig. S45 (a) The crystal structure of $\text{Li}_{6.50}\text{P}_3\text{S}_{10.25}\text{O}_{0.75}$. Here, we considered third possible Li-vacancy sites and they were labeled as numbers; (b) The relative energies of $\text{Li}_{6.25}\text{P}_3\text{S}_{10.25}\text{O}_{0.75}$ as a function of the distances between O_2 and third possible Li vacancies.

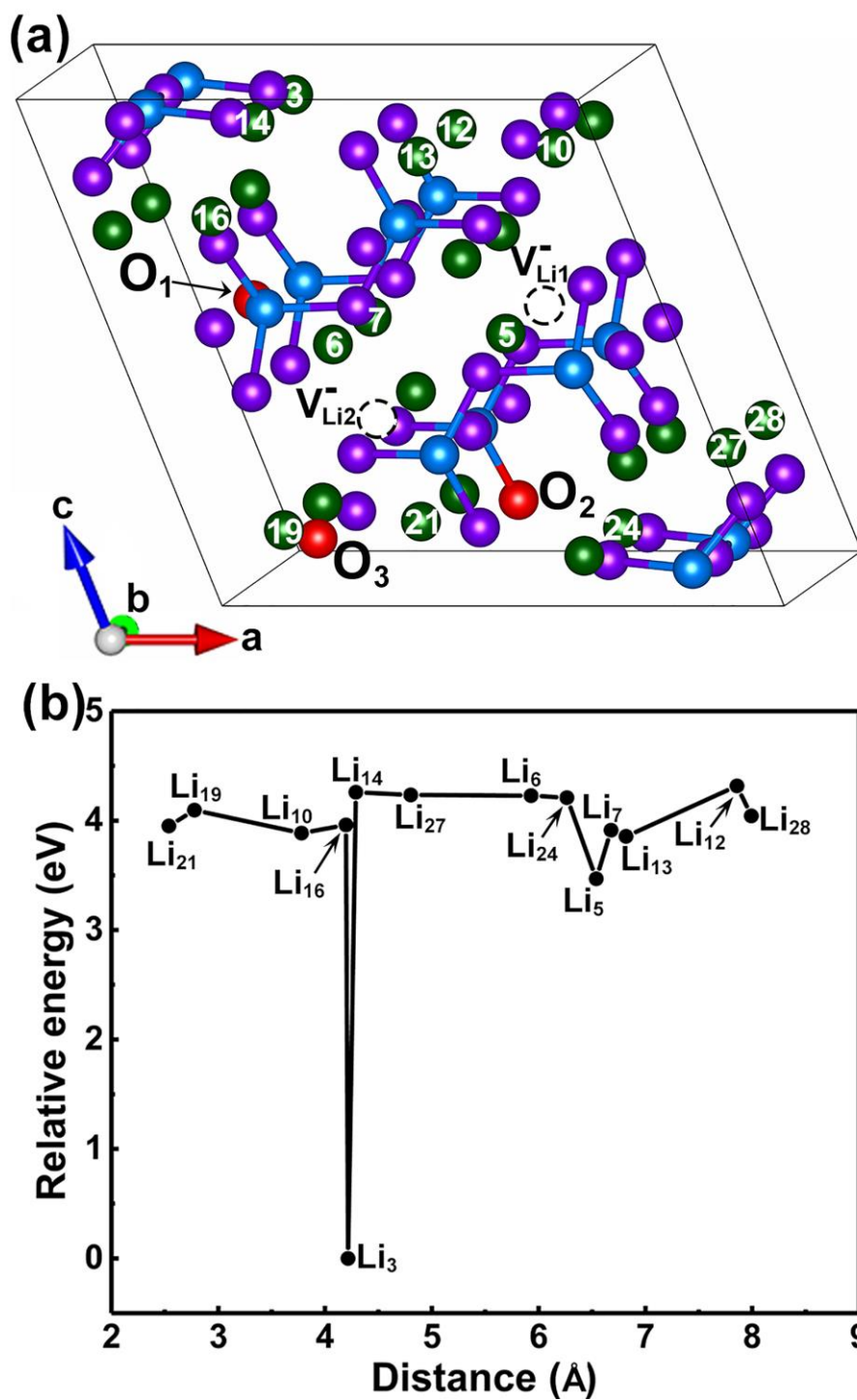


Fig. S46 (a) The crystal structure of $\text{Li}_{6.50}\text{P}_3\text{S}_{10.25}\text{O}_{0.75}$. Here, we considered third possible Li-vacancy sites and they were labeled as numbers; (b) The relative energies of $\text{Li}_{6.25}\text{P}_3\text{S}_{10.25}\text{O}_{0.75}$ as a function of the distances between O_3 and third possible Li vacancies.

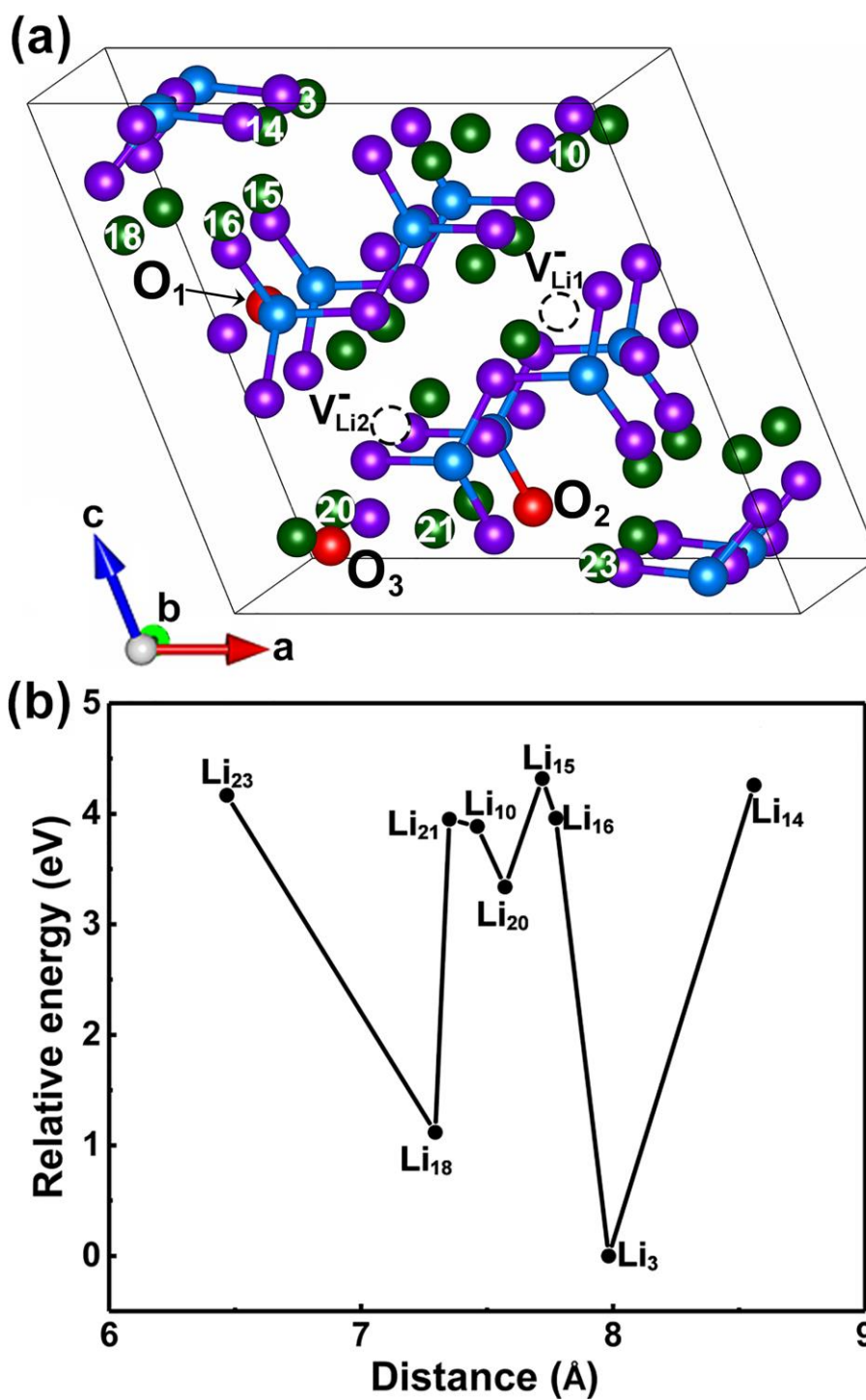


Fig. S47 (a) The crystal structure of $\text{Li}_{6.50}\text{P}_3\text{S}_{10.25}\text{O}_{0.75}$. Here, we considered third possible Li-vacancy sites and they were labeled as numbers; (b) The relative energy of $\text{Li}_{6.25}\text{P}_3\text{S}_{10.25}\text{O}_{0.75}$ as a function of the distance between possible another Li vacancy and $V_{\text{Li}1}$.

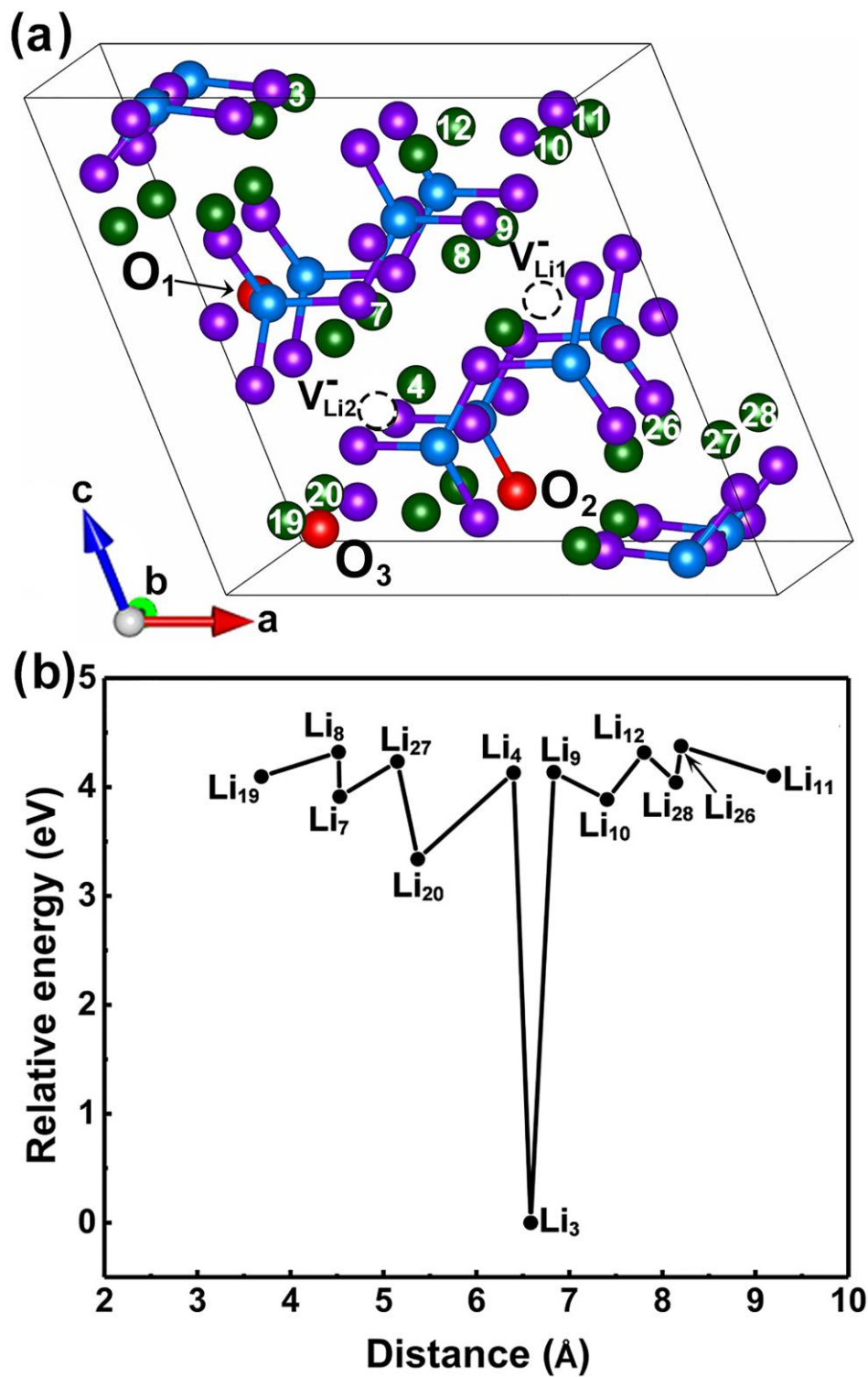


Fig. S48 (a) The crystal structure of $\text{Li}_{6.50}\text{P}_3\text{S}_{10.25}\text{O}_{0.75}$. Here, we considered third possible Li-vacancy sites and they were labeled as numbers; (b) The relative energy of $\text{Li}_{6.25}\text{P}_3\text{S}_{10.25}\text{O}_{0.75}$ as a function of the distance between possible another Li vacancy and $V_{\text{Li}2}$.

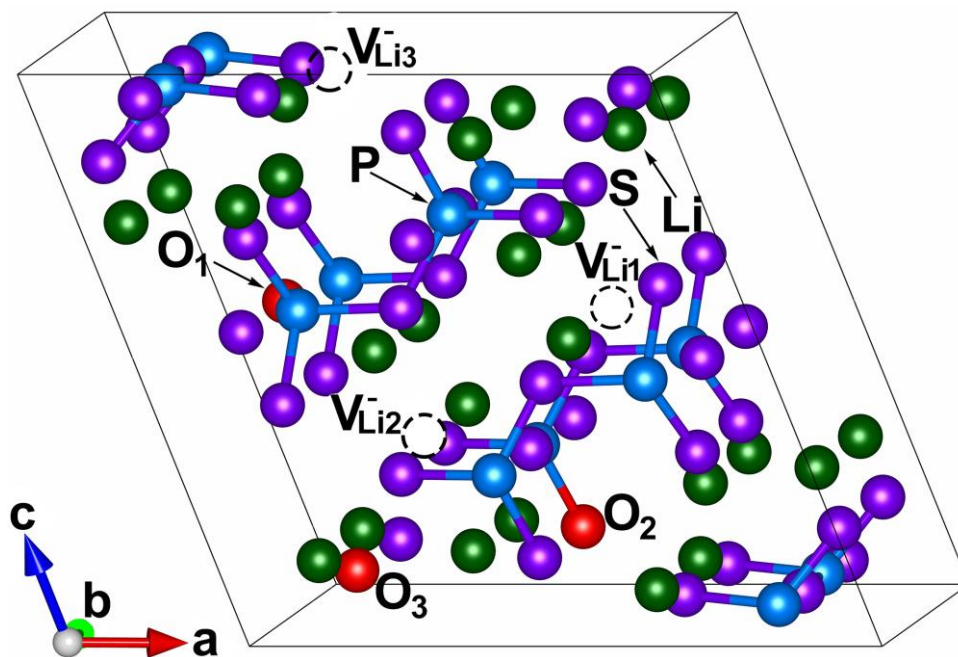


Fig. S49 Ball-and-stick model of $\text{Li}_{6.25}\text{P}_3\text{S}_{10.25}\text{O}_{0.75}$.

10. Ionic Conductivity of $\text{Li}_{7-x}\text{P}_3\text{S}_{10.25}\text{O}_{0.75}$ ($x = 0, 0.25, 0.50$ and 0.75)

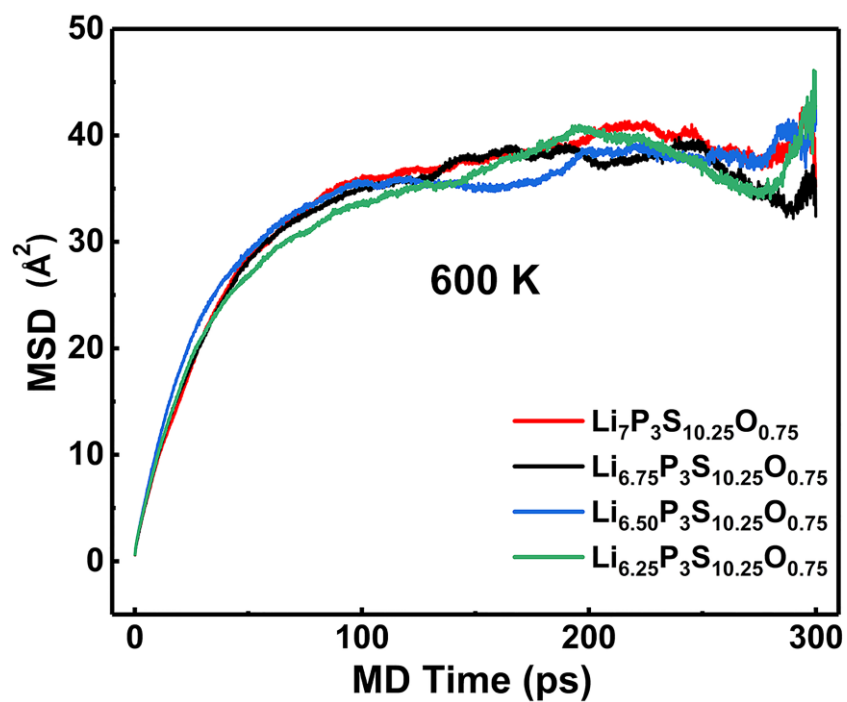


Fig. S50 Mean square displacements (MSDs) for Li, P, S and O ions in $\text{Li}_{7-x}\text{P}_3\text{S}_{10.25}\text{O}_{0.75}$ ($x = 0, 0.25, 0.50$ and 0.75) at 600 K.

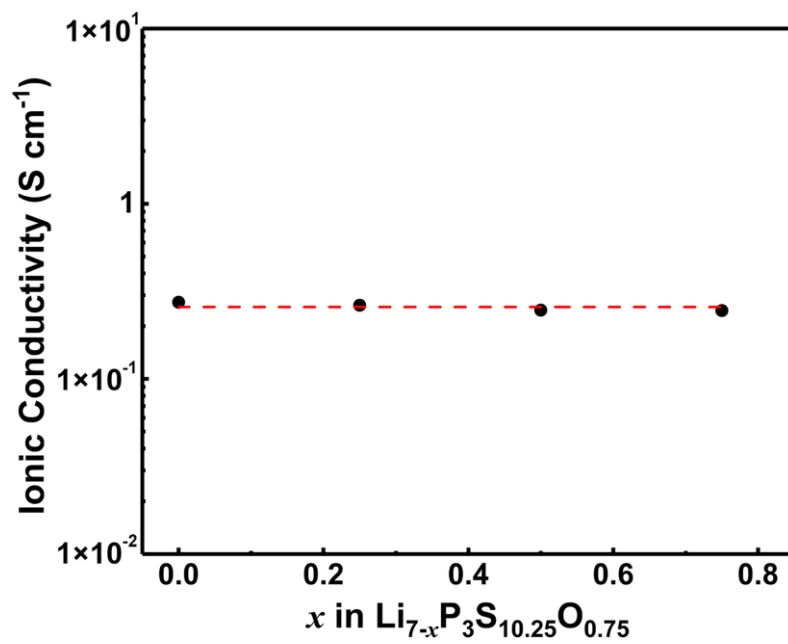


Fig. S51 Ionic conductivities for $\text{Li}_{7-x}\text{P}_3\text{S}_{10.25}\text{O}_{0.75}$ ($x = 0, 0.25, 0.50$ and 0.75) at 600 K.

11. Electrochemical Stability of $\text{Li}_7\text{P}_3\text{S}_{11}$ and $\text{Li}_7\text{P}_3\text{S}_{10.25}\text{O}_{0.75}$

Table S5. Decomposition Reactions for One Formula Unit $\text{Li}_7\text{P}_3\text{S}_{11}$

$\text{Li}_7\text{P}_3\text{S}_{11}$	
Voltage (V)	Reaction
0	$\text{Li}_7\text{P}_3\text{S}_{11} + 24 \text{Li} \rightarrow 3 \text{Li}_3\text{P} + 11 \text{Li}_2\text{S}$
0.87	$\text{Li}_7\text{P}_3\text{S}_{11} + 18 \text{Li} \rightarrow 3 \text{LiP} + 11 \text{Li}_2\text{S}$
0.94	$\text{Li}_7\text{P}_3\text{S}_{11} + 16.285 \text{Li} \rightarrow 0.4285 \text{Li}_3\text{P}_7 + 11 \text{Li}_2\text{S}$
1.17	$\text{Li}_7\text{P}_3\text{S}_{11} + 15.4275 \text{Li} \rightarrow 0.4285 \text{LiP}_7 + 11 \text{Li}_2\text{S}$
1.27	$\text{Li}_7\text{P}_3\text{S}_{11} + 15 \text{Li} \rightarrow 11 \text{Li}_2\text{S} + 3 \text{P}$
1.72	$\text{Li}_7\text{P}_3\text{S}_{11} + 1.25 \text{Li} \rightarrow 2.75 \text{Li}_3\text{PS}_4 + 0.25 \text{P}$
2.03	$\text{Li}_7\text{P}_3\text{S}_{11} + 1.077 \text{Li} \rightarrow 2.6925 \text{Li}_3\text{PS}_4 + 0.076925 \text{P}_4\text{S}_3$
2.15	$\text{Li}_7\text{P}_3\text{S}_{11} + 0.66675 \text{Li} \rightarrow 2.555 \text{Li}_3\text{PS}_4 + 0.1111 \text{P}_4\text{S}_7$
2.24	$\text{Li}_7\text{P}_3\text{S}_{11} + 0.28575 \text{Li} \rightarrow 0.14285 \text{P}_4\text{S}_9 + 2.4285 \text{Li}_3\text{PS}_4$
2.28	$\text{Li}_7\text{P}_3\text{S}_{11} \rightarrow 0.33325 \text{P}_2\text{S}_5 + 2.33325 \text{Li}_3\text{PS}_4$
2.31	$\text{Li}_7\text{P}_3\text{S}_{11} \rightarrow \text{Li}_3\text{PS}_4 + \text{P}_2\text{S}_7 + 4 \text{Li}$
2.36	$\text{Li}_7\text{P}_3\text{S}_{11} \rightarrow 1.25 \text{LiS}_4 + 1.5 \text{P}_2\text{S}_7 + 6.875 \text{Li}$
3.76	$\text{Li}_7\text{P}_3\text{S}_{11} \rightarrow 1.5 \text{P}_2\text{S}_7 + 0.5 \text{S} + 7 \text{Li}$

Table S6. Decomposition Reactions for One Formula Unit $\text{Li}_7\text{P}_3\text{S}_{10.25}\text{O}_{0.75}$

$\text{Li}_7\text{P}_3\text{S}_{10.25}\text{O}_{0.75}$	
Voltage (V)	Reaction
0	$\text{Li}_7\text{P}_3\text{S}_{10.25}\text{O}_{0.75} + 24 \text{Li} \rightarrow 10.25 \text{Li}_2\text{S} + 0.75 \text{Li}_2\text{O} + 3 \text{Li}_3\text{P}$
0.69	$\text{Li}_7\text{P}_3\text{S}_{10.25}\text{O}_{0.75} + 22.5 \text{Li} \rightarrow 10.25 \text{Li}_2\text{S} + 2.8125 \text{Li}_3\text{P} + 0.1875 \text{Li}_3\text{PO}_4$
0.87	$\text{Li}_7\text{P}_3\text{S}_{10.25}\text{O}_{0.75} + 16.875 \text{Li} \rightarrow 2.8125 \text{LiP} + 10.25 \text{Li}_2\text{S} + 0.1875 \text{Li}_3\text{PO}_4$
0.94	$\text{Li}_7\text{P}_3\text{S}_{10.25}\text{O}_{0.75} + 15.2675 \text{Li} \rightarrow 0.40175 \text{Li}_3\text{P}_7 + 10.25 \text{Li}_2\text{S} + 0.1875 \text{Li}_3\text{PO}_4$
1.17	$\text{Li}_7\text{P}_3\text{S}_{10.25}\text{O}_{0.75} + 14.465 \text{Li} \rightarrow 0.40175 \text{LiP}_7 + 10.25 \text{Li}_2\text{S} + 0.1875 \text{Li}_3\text{PO}_4$
1.27	$\text{Li}_7\text{P}_3\text{S}_{10.25}\text{O}_{0.75} + 14.0625 \text{Li} \rightarrow 10.25 \text{Li}_2\text{S} + 0.1875 \text{Li}_3\text{PO}_4 + 2.8125 \text{P}$
1.72	$\text{Li}_7\text{P}_3\text{S}_{10.25}\text{O}_{0.75} + 1.25 \text{Li} \rightarrow 2.5625 \text{Li}_3\text{PS}_4 + 0.1875 \text{Li}_3\text{PO}_4 + 0.25 \text{P}$
2.03	$\text{Li}_7\text{P}_3\text{S}_{10.25}\text{O}_{0.75} + 1.077 \text{Li} \rightarrow 2.505 \text{Li}_3\text{PS}_4 + 0.076925 \text{P}_4\text{S}_3 + 0.1875 \text{Li}_3\text{PO}_4$
2.15	$\text{Li}_7\text{P}_3\text{S}_{10.25}\text{O}_{0.75} + 0.66675 \text{Li} \rightarrow 2.368 \text{Li}_3\text{PS}_4 + 0.1111 \text{P}_4\text{S}_7 + 0.1875 \text{Li}_3\text{PO}_4$
2.24	$\text{Li}_7\text{P}_3\text{S}_{10.25}\text{O}_{0.75} + 0.28575 \text{Li} \rightarrow 0.14285 \text{P}_4\text{S}_9 + 2.241 \text{Li}_3\text{PS}_4 + 0.1875 \text{Li}_3\text{PO}_4$
2.28	$\text{Li}_7\text{P}_3\text{S}_{10.25}\text{O}_{0.75} \rightarrow 0.33325 \text{P}_2\text{S}_5 + 2.14575 \text{Li}_3\text{PS}_4 + 0.1875 \text{Li}_3\text{PO}_4$
2.31	$\text{Li}_7\text{P}_3\text{S}_{10.25}\text{O}_{0.75} \rightarrow 0.1825 \text{Li}_3\text{PS}_4 + \text{P}_2\text{S}_7 + 0.1875 \text{Li}_3\text{PO}_4 + 4 \text{Li}$
2.34	$\text{Li}_7\text{P}_3\text{S}_{10.25}\text{O}_{0.75} \rightarrow 0.045775 \text{S}_8\text{O} + 1.412 \text{P}_2\text{S}_7 + 0.17605 \text{Li}_3\text{PO}_4 + 6.4725 \text{Li}$
2.55	$\text{Li}_7\text{P}_3\text{S}_{10.25}\text{O}_{0.75} \rightarrow 0.05555 \text{S}_8\text{O} + 0.0992 \text{Li}_4\text{P}_2\text{O}_7 + 1.40075 \text{P}_2\text{S}_7 + 6.6025 \text{Li}$
2.72	$\text{Li}_7\text{P}_3\text{S}_{10.25}\text{O}_{0.75} \rightarrow 0.068175 \text{S}_8\text{O} + 1.38625 \text{P}_2\text{S}_7 + 0.227275 \text{LiPO}_3 + 6.7725 \text{Li}$
3.49	$\text{Li}_7\text{P}_3\text{S}_{10.25}\text{O}_{0.75} \rightarrow 0.0851 \text{S}_8\text{O} + 1.367 \text{P}_2\text{S}_7 + 0.132975 \text{P}_2\text{O}_5 + 7 \text{Li}$

11. References

- 1 S. P. Ong, L. Wang,; B. Kang,; G. Ceder, *Chem. Mater.*, 2008, **20**, 1798-1807.
- 2 K. Hoang, *Phys. Rev. Appl.*, 2015, **3**, 024013.
- 3 K. Minami, A. Hayashi, S. Ujiie and M. Tatsumisago, *Solid State Ionics*, 2011, **192**, 122-125
- 4 I. H. Chu, H. Nguyen, S. Hy, Y. C. Lin, Z . Wang, Z . Xu, Z. Deng, Y. S.Meng and S. P. Ong, *ACS Appl. Mater. Interfaces*, 2016, **8**, 7843-7853.
- 5 Z. Zhu, I. H. Chu, Z. Deng and S. P. Ong, *Chem. Mater.*, 2015, **27**, 8318-8325.
- 6 Z. Deng, Z. Zhu, I.-H. Chu and S. P. Ong, *Chem. Mater.*, 2016, **29**, 281-288.